Thesis

Morphological properties of the human oral mucosa - Focus on the mechanical characteristics of the maxilla region

submitted by

Sabine Otto

in partial fulfillment of the requirements for the degree of

Doktorin der Zahnmedizin

(Dr^{in}. med. dent.)

at the

Medical University of Graz

executed at the

Division of Macroscopic and Clinical Anatomy

under the supervision of

Sen. Lecturer Priv.-Doz. Dr. med. dent. **Veronica Alexandra Antipova**

Univ.-Prof. Dr. med habil. **Niels Hammer**

Univ.-Prof. Dr. med. univ. Dr. med. dent. **Norbert Jakse**

Graz, 22 July 2024

Declaration of Academic Integrity

I hereby confirm that the present diploma thesis is the result of my own independent scholarly work. I also confirm that in all cases, where material from the work of others (in books, articles, essays, dissertations, and on the internet) is acknowledged, quotations and paraphrases are clearly indicated. No material other than that cited in the reference list has been used. I have read and understood the Medical University's regulations and procedures concerning plagiarism.

Graz, 22 July 2024 Sabine Otto m.p.

Acknowledgements

First and foremost, I want to sincerely thank my supervisor, Sen. Lecturer Priv.-Doz. Dr. med. dent. Antipova, Veronica Alexandra, for her great support, valuable guidance, advice and never-ending patience throughout this research. Her support and expertise were a great help not only during this thesis but also during my medical education.

I also want to express my sincere thanks to my co-supervisors, Univ.-Prof. Dr. med. habil. Hammer, Niels and Univ.-Prof. Dr. med. habil. Jakse, Norbert for their excellent supervision, constructive feedback, and dedicated efforts, which motivated me to effectively achieve our research goals.

I would also like to thank Dr. Niestrawska, Justyna for her excellent introduction to the laboratory and machinery, which greatly enhanced my comprehension. Additionally, my sincere thanks go to Dr. Siwetz, Martin for his meticulous preparation of the mucosa, ensuring everything was perfectly set up for the experiments.

Special appreciation goes to Dr. Haspinger, Daniel. His assistance was essential and greatly contributed to the smooth progression of the research. I am particularly grateful for his thorough introduction to the laboratory and comprehensive training in equipment handling as well as assistance and proficiency during data collection and analysis.

I also want to sincerely thank the body donors and their families for generously donating their bodies for research after their passing.

Furthermore, I would like to extend my heartfelt gratitude to my friend and colleague Carolina Radetzky. Without her mutual support, this research would not have been possible. Thank you for your support, patience, and the joy that working with you has brought me.

Last but not least, I want to extend a heartfelt thank you to my entire family, especially my parents, sister and Julian. Their unwavering support made it possible for me to pursue my university education and finish this thesis. I am also very grateful to my friends as well as fellow students, who have consistently been a great source of encouragement, support and joy during these years.

Abstract in German

Insbesondere während des Kauvorgangs ist die Mundschleimhaut verschiedenen äußeren Kräften ausgesetzt. Diese Kräfte führen zu erheblichen elastischen Verformungen des Gewebes. Die Belastungs- und Verformungseigenschaften der Mundschleimhaut werden durch die Dicke des Epithels und der Menge der Kollagenfasern in der Submukosa beeinflusst. Da der Anteil älterer Menschen in der Bevölkerung weltweit zunimmt, steigt auch die Zahl zahnloser PatientInnen und damit der Bedarf an prothetischen Versorgungen. Die Mundschleimhaut unter der Prothese ist entscheidend für die Verteilung der Okklusionskräfte auf den darunterliegenden Alveolarknochen.

Die vorliegende Arbeit zielt darauf ab, die biomechanischen Eigenschaften humaner Mundschleimhaut in unfixiertem Zustand mittels Zugversuchs zu untersuchen. Dafür werden Gewebeproben aus drei verschiedenen Regionen (harter Gaumen, befestigte Gingiva und freie Mundschleimhaut) getestet, um die orts- und richtungsabhängigen Last-Verformungs-Eigenschaften zu untersuchen. Im Rahmen der Arbeit wurde die Mundschleimhaut der Oberkieferregion von 11 Individuen untersucht. Insgesamt wurden 12 Proben entnommen: 5 Gewebeproben, die die befestigte Gingiva sowie freie Mundschleimhaut enthielten, sowie 7 Gewebeproben des harten Gaumens. Zunächst wurde der Wassergehalt mithilfe des osmotischen Stressprotokolls angepasst. Anschließend wurde ein Zugversuch durchgeführt: Dabei wurden der Elastizitätsmodul, die Cauchy-Versagensspannung, die Versagensdehnung, die Versagenslast und die Querschnittsfläche berechnet und statistisch ausgewertet.

Die Ergebnisse zeigten, dass es für keinen der analysierten Parameter eine statistisch relevante Richtungsabhängigkeit innerhalb einer Region gab ($p>0,05$). Es wurde jedoch eine statistisch relevante Ortsabhängigkeit ($p<0,05$) für die Cauchy-Versagensspannung (harter Gaumen – befestigte Gingiva; freie Mundschleimhaut - befestigte Gingiva), den Elastizitätsmodul (freie Mundschleimhaut - befestigte Gingiva) sowie die Versagenslast (harter Gaumen - freie Mundschleimhaut) und die Querschnittsfläche (harter Gaumen - befestigte Gingiva; harter Gaumen – freie Mundschleimhaut) festgestellt. Hinsichtlich der Versagensdehnung wurde keine statistisch relevante Ortsabhängigkeit festgestellt ($p>0,05$).

Zusammenfassend bietet diese Arbeit erstmals verschiedene Parameter der mechanischen Belastbarkeit der intraoralen maxillären Schleimhaut auf Basis frischer (nicht fixierter) Gewebeproben. Die Ergebnisse zeigen, dass Gewebe aus verschiedenen Regionen der Mundhöhle unterschiedliche mechanische Verhaltensweisen aufweisen, welche nicht richtungsabhängig sind. Zukünftige Studien könnten dazu beitragen, die mechanischen Eigenschaften durch Gewebemorphologie, die durch histologische Analysen bestätigt wird, weiter zu untermauern.

Abstract in English

The oral mucosa is subject to various external forces, particularly during mastication. These forces lead to considerable elastic deformation of the tissue. The load-deformation properties of the oral mucosa are influenced by the thickness of the epithelium and the quantity of collagen fibers situated in the submucosa. As the ratio of elderly in a population continues to grow worldwide, the number of edentulous patients is increasing and with it the need for prosthetic restorations. The oral mucosa under the prosthesis is essential for the distribution of occlusal forces on the underlying alveolar bone.

This given study aims to investigate the stress deformation of unembalmed human oral mucosal tissue. For this purpose, tissue samples from three different regions (hard palate, attached gingiva and free oral mucosa) are tested to investigate the location and direction dependence of load-deformation properties. As part of the study, the oral mucosa of the upper jaw region of 11 individuals were examined. A total of 12 samples were taken: 5 tissue samples containing the attached gingiva and the free oral mucosa, and 7 tissue samples of the hard palate, respectively. First, their water content was adjusted with the help of the osmotic stress protocol. Then the ultimate tensile test was performed and the modulus of elasticity, the Cauchy failure stress, the failure strain, the failure load and the cross-sectional area were calculated and statistically evaluated.

The study showed that there was no statistically relevant directional dependence within a region for any of the analyzed parameters ($p>0.05$). However, a statistically relevant location-dependence ($p<0.05$) was found for the Cauchy failure stress (palate - attached gingiva; free oral mucosa - attached gingiva), the modulus of elasticity (free oral mucosa - attached gingiva) as well as the failure load (palate - free oral mucosa) and the cross-sectional area (palate - attached gingiva; palate – free oral mucosa). No statistically relevant location dependence was found with regard to the failure strain ($p>0.05$).

In summary, this study for the first time offers different parameters of mechanical resilience of the intraoral maxillary mucosa on the basis of fresh (unembalmed) samples. The results indicate that tissues from different regions exhibit different mechanical behavior that is not directional. Future studies may help substantiate the mechanical properties with tissue morphology confirmed by histological analyses.

Publication Disclaimer

Region- and direction-specific mechanical tensile properties of the human oral mucosa
Daniel Ch. Haspinger*, Sabine Otto*, Carolina Radetzky*, Justyna A. Niestrawska, Teresa M. Pirker, Martin Siwetz, Norbert Jakse, Niels Hammer[&], Veronica Antipova[&]

*These authors contributed equally to this work.
[&]These authors contributed equally to this work.

Submitted as an oral presentation, 118. Annual Meeting and Tripartite Conference of the Anatomische Gesellschaft (Graz, 25.-27.09.2024).

Table of Contents

Acknowledgements III
Abstract in German IV
Abstract in English VI
Publication Disclaimer VII
Abbreviations X
Table of Figures XI
List of Tables XII
1 Introduction 1
1.1 Topography of the oral cavity 1
1.1.1 Palate 2
1.1.2 Gingiva 3
1.1.3 Buccal mucosa 4
1.1.4 Innervation of the oral mucosa 4
1.1.5 Arteries of the oral cavity 6
1.1.6 Veins of the oral cavity 6
1.1.7 Lymphatic vessels 6
1.2 Function of the oral cavity 7
1.2.1 Sensory receptors 7
1.2.2 Reflexes of the oral cavity 8
1.3 Histology of the oral mucosa 9
1.3.1 Oral epithelium 10
1.3.2 Junction between epithelium and Lamina propria 11
1.3.3 Lamina propria 11
1.3.4 Junction between the Lamina propria and underlying tissues 12
1.3.5 Submucosa 12
1.4 Biomechanics of the oral mucosa 12
1.4.1 Static response 12
1.4.2 Dynamic response 13
1.4.3 Volumetric response 13
1.4.4 Surface interactive response 14
1.5 Preservation methods 14
1.5.1 Unembalmed specimen 15
1.5.2 Thiel embalming 15
1.5.3 Ethanol-glycerin embalming 16
1.6 Aim of the study 17
2 Materials and methods 18
2.1 Exclusion criteria and study population 18
2.2 Dissection and preservation 18
2.3 Osmotic stress protocol 19
2.3.1 Polyethylene glycol (PEG) 20
2.3.2 Preparation of the PEG concentrations 20
2.3.3 Weighing process prior to PEG immersion of specimen 21
2.3.4 PEG immersion of specimens 22
2.3.5 Vacuum protocol 23
2.3.6 Water content determination 23
2.4 Biomechanical testing group 26
2.4.1 Adjusting mucosa water content using the osmotic stress protocol 26
2.4.2 Mechanical testing 27

2.4.3 Scanning 30
2.5 Statistical analysis and processing of data 31
3 Results 32
3.1 Osmotic stress protocol 32
3.2 Biomechanical testing 33
3.2.1 Elastic modulus 33
3.2.2 Failure Cauchy stress 35
3.2.3 Failure load 39
3.2.4 Failure stretch 41
4 Discussion 44
4.1 Osmotic stress protocol: Results and comparison with previous studies 44
4.2 Mechanical testing group: Results and comparison with previous studies 45
4.3 Limitations 46
4.4 Clinical implications 47
4.5 Conclusion and future perspectives 47
References 49
Attachment 52

Abbreviations

A.g. Attached gingiva

Bp bucco-palatal

Kk Kieferkamm = maxillary crest (mc)

L.m. Lining mucosa

Mc Maxillary crest

P Palatal

PEG Polyethylene glycol

S Sagittal

Sd sinister-dexter

Tris tris(hydroxymethyl)aminomethane

V Vestibular

VPS venyl polysiloxane

Wt% weight percent

Table of Figures

Figure 1: Schematic and histological diagram of the oral mucosa (23) 9
Figure 2: Tissue sample M43: hard palate 19
Figure 3: Empty Eppendorf tube 21
Figure 4: Samples in dialysis membranes divided by clips prior to submersion into the PEG solutions 22
Figure 5: 2.5% PEG (polyethlylene glycol) time-dependent relative water content 24
Figure 6: 5% PEG (polyethylene glycol) time-dependent relative water content 25
Figure 7: 10% PEG (polyethylene glycol) time-dependent relative water content 25
Figure 8: Palatal mucosa samples L85 and L43 in dialysis membranes 27
Figure 9: 3D printed dumbbell-shaped mold 27
Figure 10: Palatal dumbbell-shaped tissue samples in the orientation "s" and "sd" 28
Figure 11: Dumbbell-shaped tissue samples of the attached gingiva and lining mucosa in the orientation "mc" and "bp" 28
Figure 12: Palatal samples M33 in 3D-printed clamps 28
Figure 13: Impression-material on palatal samples M33 28
Figure 14: Calibration process of the video extensometer 29
Figure 15: Sample clamped into the uniaxial testing machine 30
Figure 16: Sample torn by the tensile test, clamped in the uniaxial testing machine 30
Figure 17: Sample torn by the ultimate tensile test 30
Figure 18: Scan of the molds of samples L44 and L92 31
Figure 19: Comparison of 0h samples to samples submersed in 2.5%,5% and 10% PEG (polyethylene glycol) solutions for 24h 32
Figure 20: Elastic modulus (MPa) of all samples: regression method 33
Figure 21: Elastic modulus of the three regions (MPa) 34
Figure 22: Elastic modulus (MPa) of all sample groups 35
Figure 23: Failure Cauchy stress (MPa) of all samples 35
Figure 24: Failure Cauchy stress: Palatal, S 36
Figure 25: Failure Cauchy stress: Palatal, SD 36
Figure 26: Failure Cauchy stress: Lining mucosa: MC 36
Figure 27: Failure Cauchy stress: Lining mucosa: BP 36
Figure 28: Failure Cauchy stress: Attached gingiva.: MC 36
Figure 29: Failure Cauchy stress: Attached gingiva: BP 36
Figure 30: Cross sectional area: location dependency 37
Figure 31: Cross sectional area: direction dependency 37
Figure 32: Failure Cauchy stress of the three regions (MPa) 38
Figure 33: Failure Cauchy stress (MPa) of all sample groups 38
Figure 34: Failure load (N) of all samples: load vs stretch 39
Figure 35: Failure load of the three regions (N) 40
Figure 36: Failure load (N) of all sample groups 40
Figure 37: Failure stretch of all samples: load vs stretch 41
Figure 38: Failure stretch of the three regions 42
Figure 39: Failure stretch of all sample groups 42

List of Tables

Table 1: Age distribution within the study population 18
Table 2: 2.5% PEG (polyethylene glycol) time-dependent relative water content 24
Table 3: 5% PEG (polyethylene glycol) time-dependent relative water content 25
Table 4: 10% PEG (polyethylene glycol) time-dependent relative water content 26
Table 5: Overview of mean and standard deviation (ordinary one-way ANOVA) of the wt% of the native samples, as well as samples submersed in 2.5%, 5% and 10% PEG (polyethylene glycol) solutions for 24h 33
Table 6: Mean and standard deviations of elastic modulus (MPa); region dependency 34
Table 7: Elastic modulus (MPa): Mean and standard deviation (stand. d.) of all sample groups 35
Table 8: Mean and standard deviation of the cross-sectional area (mm²) of the regions palatal, lining mucosa, attached gingiva 37
Table 9: Failure Cauchy stress (MPa) of the three regions: mean and standard deviation . 38
Table 10: Failure Cauchy stress (MPa): Mean and standard deviation of all sample groups 39
Table 11: Failure load (N) of the three regions: mean and standard deviation 40
Table 12: Failure load (N): Mean and standard deviation of all sample groups 41
Table 13: Failure stretch of the three regions: mean and standard deviation 42
Table 14: Failure stretch: Mean and standard deviation of all sample groups 43

1 Introduction

The tissues of the oral mucosa are exposed to various external forces, particularly during mastication. When exposed to these forces, the oral soft tissues undergo significant elastic deformation. The thickness of the epithelium as well as the extent of collagen fibers existing in the submucosa influence the load-deformation properties of these tissues (1). In dentate patients, the masticatory muscles transfer their forces through the teeth during occlusion. By that, the vector of the forces occurring is axial to the long axis of the teeth, while to small extent forces are also directed non-axially to the contact surfaces (2). In contrast, in edentulous patients, the force generated by the masticatory muscles is mainly forwarded via the prosthesis to the underlying tissues (3). The oral mucosa then distributes these forces and by that protects the alveolar ridge (4). This causes a modification of the epithelium and connective tissue. In areas of stress, a partial damage of collagen fibers and their network was observed, which could change the tissue's resiliency and thereby have an effect on the dynamics of the tissue-denture interface (1). Constant exposure to masticatory forces could modify the oral anatomy and eventually cause inflammatory chance and remodeling of the alveolar bone (4).

1.1 Topography of the oral cavity

The oral cavity, Cavitas oris, comprises the lips, the hard palate (the anterior bony section of the roof of the mouth), the soft palate (the posterior muscular section of the roof of the mouth), the retromolar trigone (the region behind the wisdom teeth), the anterior two-thirds of the tongue, the buccal mucosa (the lining of the inner surface of the lips and cheeks), the gingiva (gums) and the area beneath the tongue known as the floor of the mouth (5). The oral cavity is the space bounded at the front by the lips and the oral fissure, at the sides by the cheeks, at the bottom by the floor of the mouth including the tongue and at the top by the hard (Palatum durum) and soft palate (Palatum molle). When the jaw is open, the oral cavity is a uniform space; when the jaw is closed, it can be subdivided into the oral vestibule (Vestibulum oris), the space between the teeth and the lips or cheeks, and the actual oral cavity, Cavitas oris propria, the space enclosed at the front and sides by the teeth and at back by the palatoglossal arch (Arcus palatoglossus) as well as the palatopharyngeal arch (Arcus palatopharyngeus), including the tonsillar fossa (Fossa tonsillaris) (6-8). In complete dentition, the oral vestibule is primarily linked to the oral cavity through the narrow

interdental spaces and the retromolar triangle (Trigonum retromolare) located between the final molar and the anterior edge of the ramus mandibulae (Ramus mandibulae) (7).

1.1.1 Palate

The palate serves as the roof of the oral cavity, providing support for the tongue and also forming the floor of the nasal cavity. It consists of the hard palate (Palatum durum) and the soft palate (Palatum molle) (8).

1.1.1.1 Palatum durum

The osseous part of the palate is formed by the incisive bone (Os incisivum), the maxilla and the palatine bone (Os palatinum), extending until approximately the level of the third molar, where it transitions into the soft palate (8).

The mucous membrane of the hard palate resembles the gum tissue and is therefore part of the masticatory mucosa. It's densely populated with small mucous glands (Glandulae palatinae) and firmly attached to the bone through robust connective tissue fibers. In the region of the median palatine suture (Sutura palatina mediana), the mucous membrane is particularly fixed. Behind the incisors, on the surface of the incisive foramen (Foramen incisivum), there is a small mucosal elevation known as the incisive papilla (Papilla incisiva). From this point, the palatine raphe (Raphe palati) extends as a weakly developed midline ridge towards the soft palate. From the anterior part of the ridge, two to five transverse palatal folds (Rugae palatinae) extend laterally, acting as rough ridges during mastication of food (7, 8).

1.1.1.2 Palatum molle

The soft palate attaches dorsally to the hard palate and comprises the velum (Velum palatinum), which includes the uvula (Uvula) dorsally. The soft palate is composed of muscle fibers and connective tissue, lined with a mucous membrane comprising a layer of stratified squamous epithelium and containing secretory salivary glands. Unlike the hard palate, the soft palate is highly flexible and lacks any bony structures. It acts as a valve between the airway and the digestive tract by raising the nasopharynx, effectively blocking communication between the Oropharynx and the Nasopharynx (8, 9).

The soft palate consists of five muscles that are vital for functions such as breathing, speech, and swallowing: the tensor veli palatine muscle (M. tensor veli palatini), levator veli palatine muscle (M. levator veli palatinie), uvular muscle (M. uvulae) as well as the palatoglossus and palatopharyngeus muscles (M. palatoglossus and M. palatopharyngeus) whose fibers converge from below into the muscular plate of the soft palate. Due to fat deposits between the glands and muscles, the soft palate is soft and deformable (8, 9).
The pharyngeal isthmus (Isthmus faucium) is formed by the base of the tongue with the lingual tonsils (Tonsilla lingualis), the soft palate with the uvula, the palatoglossal and the palatopharyngeal arch, the intervening tonsillar fossa as well as the part of the superior pharyngeal constrictor muscle that bulges during swallowing (8). The Isthmus faucium forms the posterior border of the oral cavity (10).

1.1.2 Gingiva

The gum tissue, also known as gingiva propria, is the part of the oral mucosa that belongs to the periodontium. Except for the gingival margin, it is firmly attached to the alveolar bone. Healthy gingiva follows an arc-shaped path cervical along the tooth crowns, only just covering the actual cervical region of the teeth. The interdental papillae completely fill the approximal space. Healthy gums have a pale pink, matte shiny appearance with a coarse, keratinized surface texture resembling the stippling of an orange peel. Healthy gums do not bleed upon contact (11).

The following different tissue sections of the gingiva propria are distinguished: The gingival margin, the interdental papillae and the attached gingiva. The gingival margin protrudes about 2-3 mm beyond the bony alveolar limbus. In a healthy state, it lies close and tight to the cervical tooth surface. The interdental papillae completely fill the space between the dental crown and the bony interdental septum. Due to the curved approximal surface of the teeth, a healthy interdental papilla has an oral and a vestibular part. The concavity between the facial and oral recess is called col. It is not clinically visible and varies in width and depth depending on the extent of the interproximal contact area. The attached gingiva is the part that is anchored to the cement of the tooth or the periosteum by collagen fibers. The attached gingiva is followed by the mucogingival junction (Linea girlandiformis). This junction marks the boundary between the non-movable gingiva propria and the movable vestibular mucosa, which includes the mucosa of the oral vestibule and the labial fold. The Linea girlandiformis is missing in the palatal region - here the gingiva is part of the keratinized,

non-mobile palatal mucosa (11-13). The mucosa of the lips and cheeks transitions into the gingiva at the upper or lower border of the vestibule (Fornix vestibuli) (7).

1.1.3 Buccal mucosa

The buccal mucosa is defined as the epithelial lining that covers the inner surface of the cheeks and lips, extending from the point where the opposing lips touch to the line where the alveolar ridges (both upper and lower) meet the pterygomandibular raphe (Raphe pterygomandibularis). The cheeks, like the lips, are soft tissue folds with their own structure. The muscular foundation is provided by the buccinator muscle (M. buccinator), to which the mucous membrane adheres immovably on the inside, therefore preventing it from getting between the rows of the teeth during mastication. The buccinator muscle constitutes the primary structural and functional element of the cheek. Between the buccinator and masseter muscle (M. masseter; which, along with the temporalis muscle (M. temporalis), is a powerful closer of the mouth) is the distinct, mobile buccal fat pad, known as the Corpus adiposum buccae or Bichat fat pad, which can deform under cheek pressure. Beneath the buccal mucosa are mixed salivary glands called buccal glands, and free sebaceous glands, which are not bound to hair follicles. Opposite the upper second molar, a small bump called the parotid papilla (Papilla ductus parotidei) marks the opening of the parotid duct into the oral vestibule (7, 14, 15).

1.1.4 Innervation of the oral mucosa

The oral mucosa receives its sensory innervation from the maxillary nerve (V2) and mandibular nerve (V3), the second and third branches of the trigeminal nerve (V). The trigeminal nerve also innervates the teeth and their supporting structures. Salivary glands receive secretory parasympathetic fibers from the facial nerve (VII) and glossopharyngeal nerve (IX). The motor innervation of the oral muscles mainly originates from the mandibular nerve (V3), facial nerve (VII), accessory nerve (XI), and hypoglossal nerve (XII) (7).

The skin and mucous membrane of the upper lip are supplied by the superior labial branches from the infraorbital nerve (N. infraorbitalis or V2); the skin and mucous membrane of the lower lip are supplied by the mental nerve (N. mentalis) from the inferior alveolar nerve (7).

1.1.4.1 Innervation of the lower jaw, tongue and floor of the mouth

The lower jaw's teeth and gums receive innervation from the mandibular nerve (N. mandibularis or V3). Tooth nerve supply comes from the inferior alveolar nerve (N. alveolaris inferior). The lingual gum area is mainly innervated by the lingual nerve (N. lingualis), while the labial gum area receives innervation from branches of the mental nerve (N. mentalis), a branch of the inferior alveolar nerve (N. alveolaris inferior). The buccal gum area and cheek is innervated by the buccal nerve (N. buccalis) which is also a division of the mandibular branch of the trigeminal nerve (7, 10). With regard to the general sensory innervation of the tongue and floor of the mouth, the anterior two-thirds of the tongue up to the terminal sulcus is innervated by the lingual nerve (N. lingualis), the posterior third by the glossopharyngeal nerve (N. glossopharyngeus, IX) and the transition from the base of the tongue to the epiglottis by the vagus nerve (N. vagus, X). Special sensory innervation (taste) follows a similar pattern: the anterior two thirds are innervated by the Chorda tympani branch of the facial nerve (N. facialis, VII) and the posterior third by the glossopharyngeal nerve (IX) (7).

1.1.4.2 Innervation of the upper jaw including the palate

The teeth and gums of the upper jaw are innervated by the maxillary nerve (N. maxillaris or V2). A trio of branches from the maxillary nerve, namely the anterior, middle, and posterior superior alveolar nerves (Rr. alveolares superiors anteriores, medii, and posteriores), provide innervation to the teeth. The labial and buccal gingiva are supplied by the infraorbital nerve (N. infraorbitalis or V2) and by branches of the posterior superior alveolar nerves (Rr. alveolares superiors posteriores), all of which are branches of the maxillary nerve (V2) (7). The palate's sensory innervation comes from the maxillary division of the trigeminal nerve. This division gives rise to numerous sensory branches that supply the central part of the face, including the greater and lesser palatine nerve (N. palatinus major et N. palatinus minor) as well as the nasopalatine nerve (N. nasopalatinus (V2)). The greater palatine nerve emerges from its canal through the greater palatine foramen. It courses in the palate's roof, providing sensory innervation to the gingiva and mucosa of the hard palate. The lesser palatine nerve runs parallel to the greater palatine nerve, originating from the lesser palatine foramen to supply sensory innervation to the tonsils, uvula, and soft palate (9). The nasopalatine nerve, also referred to as incisive nerve (N. incisivus), is a segment of the

maxillary division of the trigeminal nerve, which primarily supplies sensation to the anterior palate (16).

1.1.5 Arteries of the oral cavity

Various branches of the external carotid artery (A. carotis externa) contribute to the blood supply of the oral cavity, especially the maxillary artery (A. maxillaris), which is a terminal branch of the external carotid artery. The tongue receives significant vascular support from the lingual artery (A. lingualis), another branch of the A. carotis externa. The facial artery (A. facialis) provides vascular support to various structures at the floor of the mouth while the labial arteries (Aa. labiales inferior et superior), branching off the facial artery, supply blood to the lips. The hard palate is supplied by the greater palatine and superior alveolar arteries (A. palatina major and A. alveolaris superior). The alveolar arteries, originating from the terminal branches of the maxillary artery, provide blood to the gingiva and teeth in the upper jaw. Finally, the inferior alveolar artery (A. alveolaris inferior), entering the mandibular foramen alongside the inferior alveolar nerve, provides vascular support to the lower dentition and mandible (7, 10).

1.1.6 Veins of the oral cavity

Venous drainage from structures of the oral cavity primarily occurs through veins that share the same names as the accompanying arteries. The smaller veins mostly converge into the retromandibular vein (V. retromandibularis), the pterygoid plexus (Plexus venosus pterygoideus), and the facial vein (V. facialis). The retromandibular and facial veins merge and empty into the internal jugular vein (V. jugularis interna). Drainage from the tongue occurs via the lingual vein (V. lingualis), which joins the internal jugular vein. The palate is drained by the palatine vein (V. palatina), which connects to the pterygoid plexus and empties into the maxillary vein (V. maxillaris). The upper and lower lips are venously drained by the superior and inferior labial veins (Vv. labiales superior et inferior), which then join the facial vein (7).

1.1.7 Lymphatic vessels

Lymphatic vessels from the oral cavity and face predominantly converge towards the submental, submandibular, and jugulodigastric lymph nodes (Nll. submentales, submandibulares et jugulodigastrices). Lymphatic vessels originating from the molars commonly flow towards the ipsilateral submandibular lymph nodes, sometimes reaching the

jugulodigastric lymph nodes. Moreover, lymphatics from the incisors typically drain to the submental lymph nodes. Lymphatic vessels arising from the vestibular gingiva of both the maxilla and mandible typically end up in the submandibular lymph nodes, while those from the lingual and palatal gingiva often direct lymph towards the jugulodigastric lymph nodes or initially through the submandibular nodes. The lymphatic vessels originating from the soft palate typically drain into the lateral pharyngeal nodes (Nll. cervicales laterales) (7, 9). Lymph from the tip of the tongue usually drains into the submental lymph nodes, whereas lymph from the center of the tongue may drain into either the ipsilateral or contralateral submandibular lymph nodes. In the end, they drain into lymphatic nodes alongside the internal jugular vein. Finally, lymph from the posterior third of the tongue typically drains into the deep cervical lymph nodes (Nll. cervicales profundi). Since lymph drainage occurs both ipsilaterally and to the contralateral side, tumor cells in this region can be widely spread. For instance, squamous cell carcinomas, particularly those affecting the lateral edge of the tongue, frequently metastasize to the opposite side (6, 7).

1.2 Function of the oral cavity

The oral cavity plays an important role in complex motor activities, such as speaking, respiration, feeding, chewing and swallowing (17). Capturing, mastication and bolus formation of food are the main tasks of the oral cavity since it serves as the gateway to the digestive tract, where food components undergo sensory evaluation, initial mechanical breakdown by the teeth and are prepared for swallowing following the onset of food breakdown by the oral salivary glands. Thorough chewing of omnivorous food is evidently less critical for the actual digestion process in the stomach. Nevertheless, it holds significant importance for taste perception. Additionally, the formation of a cohesive food bolus triggers the swallowing reflex, which is one of the most complex reflexes involving the coordination of numerous muscles. Moreover, as a part of the respiratory system, the oral cavity facilitates the intake of large volumes of air. In addition, the oral cavity, with its various structures including the lips, tongue, teeth and palate, alongside the mimic muscles, plays a crucial role in speech production and communication. This role is emphasized by the external morphology of the mouth and the associated facial expressions (8, 18).

1.2.1 Sensory receptors

Sensory nerves linked to mechanoreceptors in the mucosal lining of the oral cavity, pharynx, and larynx are fundamental for a range of sensations. These nerves are crucial when

perceiving complex sensory experiences such as oral kinesthesia and oral stereognosis. Furthermore, they are involved in triggering reflexes and in the coordination and timing of patterned motor activities (19). The oral cavity contains the highest density of sensory receptors in the body. Taste perception is mediated by chemoreceptors located in the mucous membranes of the tongue and palate, while thermoreceptors are distributed throughout the oral mucosa. Mechanoreceptors are especially concentrated in the periodontal ligament, though their presence in the oral mucosa is less dense. As a result, the sense of touch in the teeth is more accurate than in any other area of our body. Altering the occlusion through procedures such as grinding, fillings, or crowns involves not only therapeutic considerations but also sensory-physiological challenges and limitations. Moreover, nociceptors in the endodontium are crucial for pain sensation. Unlike mechanoreceptors or thermoreceptors, the endodontium lacks such receptors, leading to pain being the only physiological response to dentin stimuli (18).

1.2.2 Reflexes of the oral cavity

The many sensory receptors in the oral cavity are the first link in the chain of reflexes that control muscles throughout the head, upper digestive system and airway. These reflexes mainly affect the set of muscles in the tongue, which are crucial for all stages of nourishment and maintaining airway patency. Some of the initial reflexes in the oral area are focused on providing nutrition. For example, the sucking reflex is only triggered at the lips during the breastfeeding period. Once breastfeeding is discontinued, such skills are quickly lost and cannot be regained. As the central nervous system matures and the oral region undergoes morphological development, new reflexes do emerge. Many of these reflexes serve to protect both the tissues within the oral cavity, such as the tongue, and the upper airway from aspiration. While basic reflexes can be elicited independently, most reflexes are integrated with more intricate oral and pharyngeal actions, such as chewing and vocalization. The initiation of the swallowing reflex occurs at the back of the tongue and the soft palate, leading to deglutition, or the act of swallowing. This process is easier for a saliva-moistened bolus than for liquid. Another reflex is the salivation reflex, also called the salivary secretion reflex, which is an automatic reaction of the body to specific stimuli, resulting in the production and release of saliva. Inflammatory conditions, the formation of stones, radiation exposure, tumors affecting the salivary glands, as well as medications and psychological factors, can significantly influence saliva production. The reflex secretion has a considerable

influence on the composition of the saliva. Finally, two protective reflexes are involved: The masticatory cessation reflex, activated by the mechanoreceptors in the periodontal ligament when there are obstacles encountered during chewing and the gag reflex, triggered by obstructions during swallowing or when there is a risk of aspiration at the transition from the oral cavity to the pharynx (17, 18).

1.3 Histology of the oral mucosa

Histologically, the oral mucosa consists of three layers: The outermost layer is a surface squamous stratified epithelium referred to as the oral epithelium. The thickness and level of keratinization of this layer vary based on the location and functional needs. Below the oral epithelium, there is the Lamina propria, which is a dense connective tissue, and further beneath lies the Submucosa, a dense irregular connective tissue containing blood vessels, glands and fat. In certain regions of the oral cavity, the Submucosa is absent, which means that the Lamina propria is bound directly to the bone or muscle (20, 21).

The structural characteristics of the oral mucosa vary considerably in different areas of the oral cavity. However, three primary types of mucosa can be distinguished based on their main functions: masticatory mucosa, lining mucosa and specialized mucosa (22). The masticatory mucosa can be found in the gingiva and hard palate, the lining mucosa, also referred to as the flexible mucosa, is present in the soft palate, the mucosa of the lips and cheeks, the oral vestibule, the alveolar mucosa as well as the floor of the mouth and the lower surface of the tongue. The specialized mucosa is found in the Dorsum linguae (21).

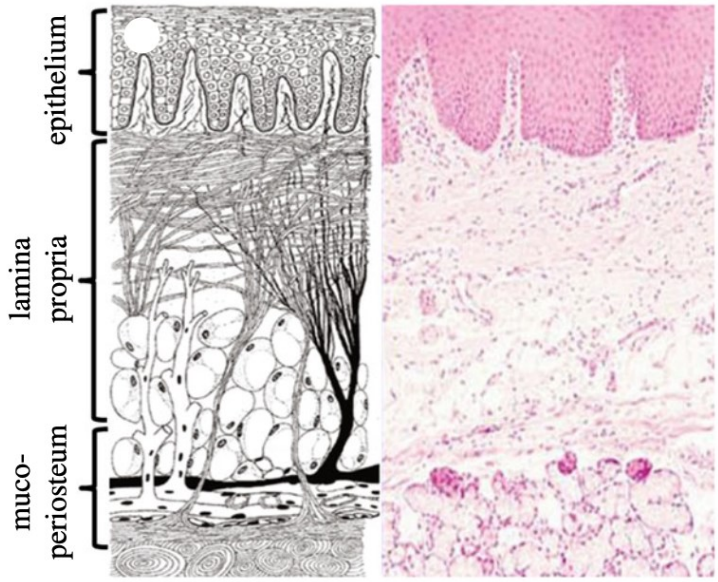

Figure 1: Schematic and histological diagram of the oral mucosa (23)

1.3.1 Oral epithelium

The oral mucosa's entire surface is lined with stratified squamous epithelium. This tissue is well-organized, semipermeable, avascular, and with its thickness and degree of keratinization varying based on its location in the oral cavity and the functional and mechanical demands of that specific area. The surface of the oral epithelium exhibits varying levels of keratinization. It ranges from no keratinization, as seen in the cheek, to partial or parakeratinization, sometimes found on the gingiva and some areas of the palate. Full or orthokeratinization is present in most areas of the hard palate and on the gingiva where it is firmly bound to the bone. Keratinized areas are considered masticatory mucosa, while non-keratinized areas are considered lining mucosa. The oral epithelium protects the oral cavity from microbial, mechanical and chemical damage. The epithelium sits on a basement membrane that divides it from the connective tissue and is made up of tightly packed epithelial cells that exhibit different levels of differentiation: It starts with the deepest basal layer of undifferentiated cells that continuously divide and progresses through layers of suprabasal cells, which undergo different morphological and biochemical changes, depending on the specific region and type of mucosa (20, 21, 24).

1.3.1.1 Epithelium of the masticatory mucosa

The oral epithelium in keratinized oral mucosa is composed of four layers. Starting from the deepest layer, these are the Stratum basale, which is followed by the Stratum spinosum, Stratum granulosum, and finally the Stratum corneum (20). The Stratum basale consists of a layer of columnar or cuboidal cells positioned above the basement membrane, to which they are attached by hemidesmosomes. These cuboidal or columnar cells are notable because of their capacity of mitosis. Directly above the Stratum basale is the Stratum spinosum, formed by several layers of larger, spiky-shaped cells known as prickle cells. The Stratum spinosum is rather thick and forms the largest part of the epithelium. It is followed by the stratum granulosum, which contains cells with small cytoplasmic keratohyalin granules. There are at least two types of granules: one, that is found in highly keratinized parts of the epithelium, which is also found in skin epithelium, which is characterized by its irregular shape and the high electron dense; and another that is less irregular and can be found in non-keratinizing as well as keratinizing epithelium. The outermost layer is the Stratum superficiale or Stratum corneum, which is a keratinized layer of very flat, condensed cells

with a thickened cell membrane. Here a drastic chance in the structure of the cells is noticed as they are nucleus-free and neither granules, nor organelles can be found (20, 24).

1.3.1.2 Epithelium of the lining mucosa

The non-keratinized epithelium found on the lining mucosa does not contain a granular layer, and the spinous layer is typically thinner in comparison to the keratinized epithelium. It is less resistant to damage but can be stretched, possesses a basal layer resembling that of masticatory mucosa, with the additional presence of cytokeratin. Similar alterations take place in the cells as they progress and transform into the Stratum spinosum, including enlargement and alteration in morphology. Cells in the outermost layer, the Stratum superficiale, also show an increase of the thickness of their membrane, just like those of the keratinized epithelium. However, the permeability in non-keratinized mucosa is higher than in keratinized mucosa. Although the nuclei remain present in this layer, there is a gradual reduction in organelle volume and a decrease in desmosomes, leading to desquamation of the cells (20, 21).

1.3.1.3 Epithelium of the specialized mucosa

Specialized oral mucosa is located on the tongue's dorsal surface and comprises keratinized structures such as filiform papillae, and the dorsal surfaces of fungiform and circumvallate papillae, alongside non-keratinized, interpapillary regions (21).

1.3.2 Junction between epithelium and Lamina propria

The epithelium is connected to the connective tissue beneath by an area of basement membrane. The structure of this junction changes based on the type of oral mucosa and is influenced by the tissue's functional needs. The ratio between the height of the connective tissue papillae and the thickness of the epithelium tends to remain consistent across different areas of the oral mucosa. The junctions' heights vary from 0.6 mm to 0.74 mm, except the floor of the mouth at 0.3 mm. In masticatory mucosa, approximately 1.5-2.5 times more papillae per mm^2 can be found compared to the lining mucosa. This is due to the forces during mastication exerted on the mucosa (21).

1.3.3 Lamina propria

The superficial dense connective tissue, also referred to as Lamina propria, gives support to the overlying epithelium (21). It comprises nerves, blood vessels, various cells including

macrophages, fibroblasts, mast cells and inflammatory cells along with fibers, which are all suspended in a gel-like substance composed of proteoglycans and glycoproteins (20). There is limited regional diversity observed in the connective tissue of the oral mucosa, although elastic fibers exist in the connective tissues of the lining mucosa and the arrangement of collagen fibers is less uniform. The superficial layer of the Lamina propria is called papillary layer (since it's composed of connective tissue papillae), deeper down one can find the reticular layer, which gets its name due to the fiber network present (21).

1.3.4 Junction between the Lamina propria and underlying tissues

The connection between the reticular layer of the Lamina propria and the underlying tissues varies according to the type of mucosa. In anterior sections of the hard palate and the gingiva, the Lamina propria is anchored to the periosteum and teeth, while in the posterior-lateral parts of the hard palate, it is attached to a fibrous submucosa, which contains fat and salivary glands. The Lamina propria of the lining mucosa is connected to the submucosa (21).

1.3.5 Submucosa

The submucosa is an elastic and fibrocollagenous tissue which contains blood vessels and nerves. Depending on its location, minor salivary glands, lymphoid tissue, fat as well as muscle may be included in this layer. The submucosa is present in all areas of the buccal cavity except the attached gingiva and parts of the hard palate. There, without any intervening submucosa, the oral mucosa is directly connected to the periosteum of the underlying bone. This arrangement is referred to as the Mucoperiosteum, providing a firm, inelastic attachment to the bone (20, 22).

1.4 Biomechanics of the oral mucosa

The oral mucosa is crucial in distributing occlusal forces to the underlying bony ridge during mastication. It has a number of different biomechanical responses; however, there are four primary biomechanical issues that are crucial to clinical applications, offering significant biological insights into these mechanical models. These four include static response, dynamic response, volumetric response and surface interactive response (4).

1.4.1 Static response

Static response is a form of short-term or instant response, which refers to the path-dependent elasticity of a material (4). The modulus of elasticity is a fundamental parameter that

describes how a material deforms in response to an applied force. The oral mucosa is known to be highly deformable under compression, and its elastic modulus varies widely. As a heterogeneous material, the immediate stiffness of the mucosa is influenced by both its solid matrix structure (such as the epithelial layer and its fibrous network, as well as blood vessels etc.) and its fluid components (1).

1.4.2 Dynamic response

Besides its immediate elastic reactions, the oral mucosa also demonstrates a time-dependent dynamic response under loading and unloading, known as creep and delayed recovery. The dynamic response is explained by the viscosity component, often assuming the mucosa tissue is uniform. The diversity within the mucosa has not been thoroughly investigated, but biomechanically, this diversity influences interstitial fluid activity and the related dynamic response, thereby linking microscopic biomechanics to physiology. In the elderly population, the mucosa typically exhibits more pronounced viscous behavior and less rebound with slower recovery due to the decreased amount of elastin and they tend to have an enhanced ability to retain fluid in the mucosa. Larger contact areas usually lead to firmer mucosal responses; higher loading rates produce comparable effects. From literature, male subjects appear to more frequently display a stiffer mucosal response with slower recovery compared to female subjects, probably because females typically have thicker mucosa than males (4, 25).

1.4.3 Volumetric response

The volumetric response describes the mucosa's ability to handle volume changes during shape alteration. This response is influenced by the Poisson ratio, which is also known as compressibility or lateral response (4). It represents the negative ratio of transverse to longitudinal stretch. Under compression, the mucosa tends to expand sideways perpendicular to the compression source, while it contracts under tension. The Poisson ratio varies for each individual and is influenced by factors such as mucosal location, thickness, morphology, age, and how long dentures have been worn. Determining the Poisson ratio is vital for estimating how contact pressure and displacement distribute across the oral mucosa under removable dentures, which eventually helps prevent tissue damage caused by compression and shearing forces (26).

1.4.4 Surface interactive response

The surface interaction is characterized by the friction coefficients between the mucosa and the denture (4). The friction coefficient is affected by the physiological condition of the mucosa, for example by xerostomia. Well-hydrated oral mucosa has a lower friction coefficient compared to mucosa with xerostomia. Additionally, the denture's material and the amount of saliva influence the friction coefficient. Therefore, calculating the friction coefficient requires considering each individual's physiological condition and the denture material used. Properly determining the friction coefficient helps prevent mucosal trauma, such as irritation and keratosis, caused by denture friction (26).

1.5 Preservation methods

Throughout history, various methods of embalming have been devised to prevent specimens from undergoing decomposition and autolysis (27, 28). Embalming fluids should achieve long-term structural preservation without causing excessive hardening of the tissue, preserve the natural color, and ensure durability of the tissues over time (29, 30). In medical education and research, preserved human tissue is frequently substituted for unembalmed human tissue, primarily due to availability and ethical considerations. Emerging preservation techniques like the Thiel method offer the potential for more lifelike mechanical characteristics compared to traditional formaldehyde fixation (28). Because of protein crosslinking, formalin fixation produces stiff specimens that do not closely mimic the properties of unembalmed tissue. Hence, this embalming method is unsuitable for preclinical biomechanical assessments. A more promising embalming technique for biomechanical studies is the soft-fix method, initially introduced by Thiel in 1992 (31). The Thiel embalming method incorporates a lower concentration of formaldehyde compared to the typical formalin-based solutions (32). Formaldehyde has been categorized as carcinogenic for humans (28). Ethanol-glycerin as a fixing agent and thymol as a preservative offer viable alternatives to formaldehyde and phenol, without posing significant health risks. Their use provides robust specimens while maintaining tissue flexibility and aesthetic appearance (27). Previous studies have shown that ethanol-glycerin embalming was rated higher regarding tissue preservation and suitability in anatomical dissection, whereas Thiel embalming was found to provide better tissue pliability (29).

1.5.1 Unembalmed specimen

The challenges of obtaining fresh tissue and the lengthy experimental testing process often require a storage method that may compromise functional properties (33). Refrigeration and freezing are commonly used to preserve experimental soft tissues. Studies have shown that there is no significant difference observed in the physiological, sub-failure, and ultimate failure mechanics between fresh and frozen specimens. Nevertheless, the mechanical properties may be influenced by short-term tissue refrigeration (34).

1.5.2 Thiel embalming

The Thiel method, often referred to as "the preservation of the whole body with natural color" by its creator, strives to achieve more authentic material properties when compared to previously employed embalming methods (28). Thiel-preserved specimens have remarkably realistic visual and haptic characteristics (35). The Thiel's method involves an initial injection of two infusion solutions into the body, followed by immersion in the solution in movable, custom-made containers for approximately 6-8 months. Initially, 15.0 liters of the Thiel fixative are injected into the arterial system. The injection solution comprises a stock solution (containing 2 kg of ammonium nitrate, 300 g of boric acid, 500 g of potassium nitrate, and 3 liters of ethylene glycol dissolved in 10 liters of hot water; with a pH of 3.5), a p-chlorocresol solution (comprising 0.03 kg of p-chlorocresol and 0.5 liters of ethylene glycol dissolved in 0.5 liters of distilled water), 0.3 liters of formaldehyde, and 0.7 kg of sodium sulfide. Following donor registration, cleaning, and shaving of the body, the femoral artery is located and two cannulas are inserted—one cranially towards the external iliac artery and the other caudally towards the popliteal artery. Then, the fixative is injected at a maximum pressure of 0.5 bar using a pump (28, 35). Typically, the injection takes 6 to 10 cycles, each lasting 10 minutes, with interruptions lasting two hours or longer to ensure even distribution of the fixative. On average, the injection process takes around 24 hours. The injection process is deemed complete when the keratin of the epidermis and the nails begin to detach. Then the second fixation stage, involving the submersion into the solution in containers, takes place. The containers are filled with Thiel container solution, consisting of 20 kg of ammonium nitrate, 6 kg of boric acid, 190 g of p-chlorocresol, 22 liters of ethylene glycol, 4 liters of formaldehyde and 10 kg of potassium nitrate. All these ingredients are then dissolved in 200 liters of hot tap water (35).

Thiel-preserved specimens have remarkably realistic visual and haptic characteristics (35). It serves as an alternative to the use of fresh frozen specimens when investigating some biomechanical principles/mechanisms. Some Thiel-embalmed specimens show an inverse trend in elastic modulus, which may be related to slight differences in embalming, which means that caution should be exercised when using Thiel-embalmed specimens to obtain raw numerical data for direct clinical application (31). In addition, Thiel-preserved specimens are not suitable for determining the elastic modulus or the ultimate stress of tendons and ligaments, as the boric acid and formaldehyde present can alter these values compared to unfixed tissue samples. Shrinkage artifacts and the decellularization due to Thiel fixatives may also negatively impact tissue biomechanics and morphometry. Furthermore, the histology of Thiel-preserved specimens is rather poor, since it changes the tissue's structure at cellular level, e.g. by showing fiber fragmentation as well as lack of nuclei (35, 36).

1.5.3 Ethanol-glycerin embalming

A mixture of ethanol and glycerin, at a ratio of 0.7 L/kg body weight, is injected in an explosion-proof room. Glycerin is added at a ratio of 2 to 10%, based on the donor's physical condition (35). The mixture is injected into the femoral artery through two cannulas: one pointing upwards and the other downwards. The ethanol-glycerin fixative is administered with a pump at a maximum pressure of 0.5 to 0.8 bars, depending on the state of the vascular system. Injection is paused for two hours when the abdominal wall begins to swell, with longer or overnight pauses possible to ensure proper distribution of the fixative. This process is repeated six to ten times until the distal extremities show increased turgor from the ethanol-glycerin. The injection procedure generally takes around 36 hours. The bodies are then immersed in metal containers filled with a water-diluted ethanol solution (65% by volume) to preserve the skin. They remain in these containers for an average of four weeks. For long-term storage, the bodies are wrapped in cotton cloths and polyethylene foil. Cooling the specimens to 3 to 5°C preserves the fixed bodies for a minimum of three years. To maintain fixation at room temperature, an alternative preservation method is utilized: a thymol-ethanol solution. This solution is prepared by mixing 300.44 g (2 mol) of thymol powder with 1 L of ethanol, which is then diluted with 10 L of water to achieve a final concentration of 3% thymol (0.18 mol/L). The thymol solution is applied to moisten the specimens and prevent bacterial or fungal contamination (27).

Ethanol-glycerin-fixed specimens show significantly less joint motion compared to those fixed with Thiel solution or unfixed tissues. Despite this reduced range of motion, ethanol-glycerin fixation enables dissection of extremities in an abducted position without damaging nearby muscles. However, when compared to formaldehyde-fixed specimens, specimens fixed with ethanol-glycerin exhibit better rigidity, color retention, and range of joint motion. Histological specimens can be effectively obtained and stained from ethanol-glycerin fixed tissues, with results similar to those from tissues initially fixed with formaldehyde. Concerning the biomechanical properties of ethanol-glycerin fixed tissues, the same recommendations apply as for those fixed with formaldehyde or Thiel solution. Ethanol significantly alters the material properties of soft tissues like tendons or ligaments during uniaxial testing, likely due to denaturation of the proteins' tertiary structures. This alteration may be reversible by rinsing the tissues; however, bone samples were altered irreversibly, likely because the bone's organic components were changed by ethanol (35).

1.6 Aim of the study

The aim of the given study was to evaluate the mechanical properties of the mucosa in the maxilla region. The elastic modulus, failure Cauchy stress well as failure load and failure stretch of fresh-frozen human oral mucosa tissues of the maxillary region will be assessed. The focus was placed on the differences concerning directional and locational dependency. The primary null hypothesis was that there is a location dependency with regard to the parameters mentioned above between the different sites of the upper jaw tested: hard palate, lining mucosa and attached gingiva. The secondary null hypothesis was that there was a directional dependency regarding the mechanical properties within these three regions.

2 Materials and methods

The study was approved by the Ethics Committee of the Medical University of Graz, protocol number 35-500 ex 22/23. Between April 2022 and May 2022, the oral mucosa of the maxilla region of 11 body donors following their death were dissected and frozen at -80 °C. All body donors were bequeathed to the Division of Macroscopic and Clinical Anatomy of the Medical University of Graz (Austria) under the approval of the ongoing body donation program of the Medical University of Graz and in accordance with the Styrian Death and Funeral Act. The osmotic protocol as well as biomechanical testing of the oral mucosa was performed from February 2024 to May 2024. All specimens were preserved by shock-freezing at -80 °C (37, 38). Prior to the biomechanical testing and the osmotic stress protocol being performed on samples of the human oral mucosa, test trials were performed: The osmotic as well as the vacuum protocol were performed first on a sponge cloth, later on a muscular tendon. The biomechanical test trial was performed on a medical glove.

2.1 Exclusion criteria and study population

The body donors for the present study had an edentulous or partially dentate maxilla. The study population consisted of 11 body donors: seven of them being female, and four being male. On average, the body donors were 81.9 years old.

	Average	Maximum	Minimum
Age in years	81.9	91	70

Table 1: Age distribution within the study population

2.2 Dissection and preservation

The oral mucosa of the upper jaw was dissected from 11 specimens from three different regions: the hard palate, the attached gingiva as well as the lining mucosa. The samples were then marked based on their localization in the oral cavity by using surgical suture in different lengths: Short-short meant right, long-long meant left, short-long meant anterior. After that, the samples were divided into two main groups by region: on the one hand the hard palate and on the other the attached gingiva as well as the lining mucosa of the upper jaw. A total of 12 samples were obtained: 5 tissue samples including the attached gingiva and lining

mucosa and 7 tissue samples of the hard palate. The samples were then shock-frozen at -80°C (38).

Prior to the osmotic stress protocol, 10 small samples each of the 12 tissue samples each were dissected. Ten samples each were needed in order to perform the osmotic stress technique in 3 different polyethylene glycol (PEG) concentrations at 3 different times. A tenth sample each was needed in order to serve as a control to determine the initial water content of the oral mucosa in fresh condition (39).

Figure 2: Tissue sample M43: hard palate

2.3 Osmotic stress protocol

The osmotic stress technique was performed to exclude any change in the mechanical properties of the oral mucosa due to its water content. The aim was to adjust the water content to their native value. In order to achieve that, polyethylene glycol (PEG; Rotipuran, Carl Roth GmbH + Co. KG, Karlsruhe, Germany; molecular weight 20.000 Da) was prepared at a 2.5 wt%, 5 wt% and 10 wt% concentration, buffered with 20mM Tris (Pufferan, Carl Roth GmbH + Co. KG, Karlsruhe, Germany; molecular weight 121.14 Da). After dissecting ten small samples each of the twelve tissue samples used for the osmotic stress protocol, first the water content of the control group was determined by freeze-drying. After that, the water content of the samples after submersion in three different PEG concentrations at three different times was assessed (39).

2.3.1 Polyethylene glycol (PEG)

The aggregate state and the specific properties of PEG are strongly related to the size of the PEG molecule. Molecular masses of 1000 and above are solid substances. In the experiment, PEG with a molecular mass of 20.000 Da was used, which means that it is a white to almost white, solid substance with a waxy or paraffin-like appearance. One of the special properties of low molecular weight polyethylene glycols is their amazing solubility in water as they can be mixed with water in any ratio. This water solubility decreases with increasing molecular weight, but even at a molecular weight of 35,000 g/mol, 50% aqueous solutions can be prepared at room temperature (40). Polyethylene glycol hydrogels are widely used as customizable substrates in both biological and technical fields due to their excellent biocompatibility and remarkable hydrophilicity. Because of their advantageous material properties such as transparency, flexibility, biocompatibility, and permeability to gases and nutrients, PEG hydrogels find extensive use in biomedical applications. These include serving as artificial tissue scaffolds, matrices for controlled biomolecule release, wound dressings, and contact lenses (41). In the experiment, the PEG solutions were used to perform the osmotic stress technique by adjusting the samples' water content (39).

2.3.2 Preparation of the PEG concentrations

The aim was to mix three different PEG concentrations: 2.5 wt%, 5 wt% and 10 wt% with a pH value of 7 (39). This pH value was used because it corresponds to the pH value of saliva (42).

The first step was the 3-point calibration of the pH meter (EC-31 pH, Phoenix Instrument GmbH, Garbsen, Germany). For this purpose, the pH electrode was calibrated using three standard buffers (Technical Buffer pH 4.01; pH 7.00; pH 10.01, Xylem Analytics Germany Sales GmbH & Co. KG, Weilheim, Germany). Buffer solutions should be chosen so that the pH of the unknown is within the range of the standards. In between the calibrations in three different pH concentrations, the electrode was washed with distilled water and gently blotted dry using a tissue (43).

After the calibration process, the PEG (molecular weight 20.000 Da) solutions in concentrations of 2.5 wt%, 5 wt% and 10 wt% were prepared. The PEG was dissolved in an isotonic sodium-chloride solution, buffered with 20 mM Tris (hydroxymethyl

aminomethane; pH = 7) (39). The aim was to have 2 liters of each PEG solution. The molar mass (M) of Tris is 121.14 g/mol (44). Using the amount of substance formula, n=m/M, the amount of Tris was calculated (45):

$$n = \frac{m}{M} = \frac{m}{121{,}14}$$

$$n = 20\ mM\ /L$$

$$m = 0{,}02\ \times 121{,}14$$

$$m = 2{,}4228\ g\ /L \rightarrow 4{,}845\ \text{g Tris/2L}$$

For the 5 wt% PEG solution of 2 liters, 200 ml isotonic sodium-chloride was mixed with 4.845 g Tris and 100 g PEG. Then, 1.7 liters of distilled water was added and the solution was mixed on a magnetic stirrer until the particles had completely dissolved. This process took 20 minutes. After that, the pH was measured (46). As it was above pH 7, hydrochloric acid (HCl, 3N) was added until the desired pH of 7 was reached (47). After checking the pH again, the PEG concentration was stored at 4°C (39).

2.3.3 Weighing process prior to PEG immersion of specimen

In order to be able to weigh the tissue samples and determine their water content by freeze-drying in the later course of the experiment, tubes (Eppendorf Tubes® 5.0 mL, Eppendorf SE, Hamburg, Germany) were first labelled and weighed when empty. A small hole was drilled in the tubes' cap to allow water to escape during the freeze-drying process before weighing (38).

Figure 3: Empty Eppendorf tube

To determine the exact weight of the samples, a precision scale (Quintix®, Sartorius Lab Instruments GmbH & Co. KG, Göttingen, Germany) was used. The Sartorius Quintix

laboratory balance has a maximum weighing capacity of 210 g and a readability of 0.1 mg (48).

Once all the empty Eppendorf tubes had been weighed, the frozen 0-hour samples were placed in the corresponding Eppendorf tubes. Then their weight prior to freeze-drying was defined in order to serve as a control for the determination of the initial water content of the oral mucosa in fresh state. These samples were then stored at -80°C until the osmotic stress protocol was finished (39).

2.3.4 PEG immersion of specimens

In order to submerse the samples into the different PEG solutions, dialysis membranes (Carl Roth GmbH + Co. KG, Karlsruhe, Germany; molecular weight cut-off = 6000–8000 Da) were used (39).

A total of 108 samples (9 small samples each of the 5 samples of the buccal mucosa as well as attached gingiva and 7 samples of the hard palate) were enclosed within 42-mm dialysis membranes (Spectra/Por molecularporous membrane tubing, Carl Roth GmbH + Co. KG, Karlsruhe, Germany; molecular weight cut-off = 6000–8000 Da), sealed and divided into compartments for each individual sample at both ends using clips, and immersed in 2.5 wt%, 5 wt% and 10 wt% PEG solutions for durations of 8, 12 and 24 hours at 4°C, under continuous stirring of the PEG solutions. After being submerged in the PEG solutions for the given times, the samples were taken out of the dialysis membranes and placed in the previously prepared tubes in order to be weighed again (39). The filled tubes were then stored again at -80°C before freeze-drying (38).

Figure 4: Samples in dialysis membranes divided by clips prior to submersion into the PEG solutions

2.3.5 Vacuum protocol

After all the samples underwent the osmotic protocol, these samples as well as the control group were lyophilized for a minimum of 48 hours (39). Freeze-drying, also known as lyophilization, is defined as sublimation of ice under vacuum (49). It allows the volume of water to be measured by extracting all water from the tissue (50). In normal atmospheric conditions, the transformation of liquid water into vapor through heating is referred to as evaporation. However, at the triple point, all three states of water - solid (ice), liquid, and gas (vapor) - can exist simultaneously, demonstrating that under subatmospheric pressures, ice can transition directly into vapor via sublimation. The sublimation of ice from a frozen sample yields an open, porous, and dry structure. Unlike evaporation, which results in the concentration of components as drying proceeds, sublimation under vacuum reduces concentration effects, yielding a dry product that is active and easily soluble. To sustain freeze-drying conditions, it is important to decrease the partial pressure of water below the triple point (approximately 800 mBar at 0°C) to ensure the direct transformation of ice into water vapor. Reducing the chamber pressure accelerates the rate of sublimation by lowering the concentration of gas/vapor above the sample, thereby minimizing resistance to water molecules migrating from the sample (49).

Freeze-drying is a three-stage process: Freezing, primary drying and secondary drying. After being adequately frozen, the samples undergo the primary drying phase, which means sublimation of the ice. Once primary freeze-drying concludes and all ice has sublimated, there remains bound moisture within the product. Although the product may seem dry, its residual moisture content could be as high as 7-8%. Further drying at elevated temperatures is required to decrease the residual moisture content to optimal levels. During secondary drying, the remaining water is more tightly bound, necessitating more energy for its removal. Traditionally, reducing the chamber pressure to the highest achievable vacuum level has been considered advantageous for promoting the desorption of water (51). In the experiment, the Eppendorf tubes containing the frozen tissue samples were taken out of the freezer (-80°C) and immediately put into the vacuum pump at a room temperature of 22°C.

2.3.6 Water content determination

After the lyophilization process, all samples were weighed in their corresponding Eppendorf tube again. In order to determine the samples' net weight and therefore calculate their water content, the Eppendorf tubes' empty weight was subtracted from the weight before and after

the freeze-drying process. After that, each samples' water content was calculated using the following equation:

$$Rel.water\ content\ (\%) = \frac{m_{wet} - m_{dry}}{m_{wet}} \times 100$$

2.3.6.1 Determination of the appropriate PEG concentration

The control groups' average water content was 70.8%, with a median of 73.5% and a standard deviation of 10.1%. As the aim was to adjust the water content to their native value, precisely the water content of the control group, the time dependent decrease of water content related to a specific PEG concentration had to be determined (39). The calculated water content of the tissue samples at a given time in 2.5 wt%, 5 wt% and 10 wt% PEG concentrations can be seen in Tables 2-4 as well as Figures 5-7.

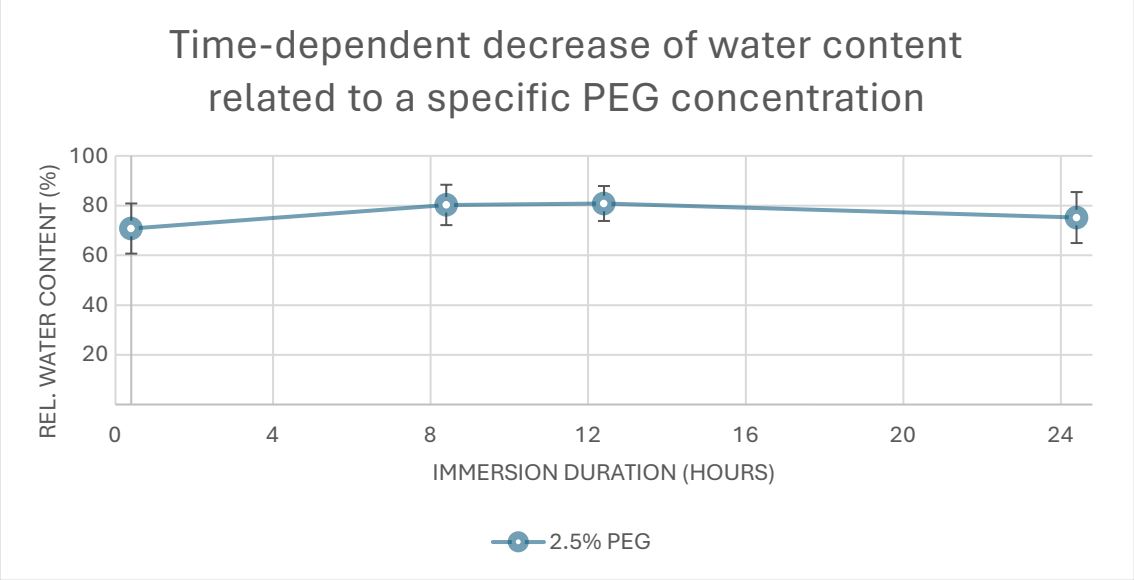

Figure 5: 2.5% PEG (polyethlylene glycol) time-dependent relative water content

		0h	8h	12h	24h
Relative water content [%]	Median	73.46	82.10	78.88	77.73
	Mean	70.78	80.27	80.85	75.20
	Standard deviation	10.09	8.12	7.03	10.25

Table 2: 2.5% PEG (polyethylene glycol) time-dependent relative water content

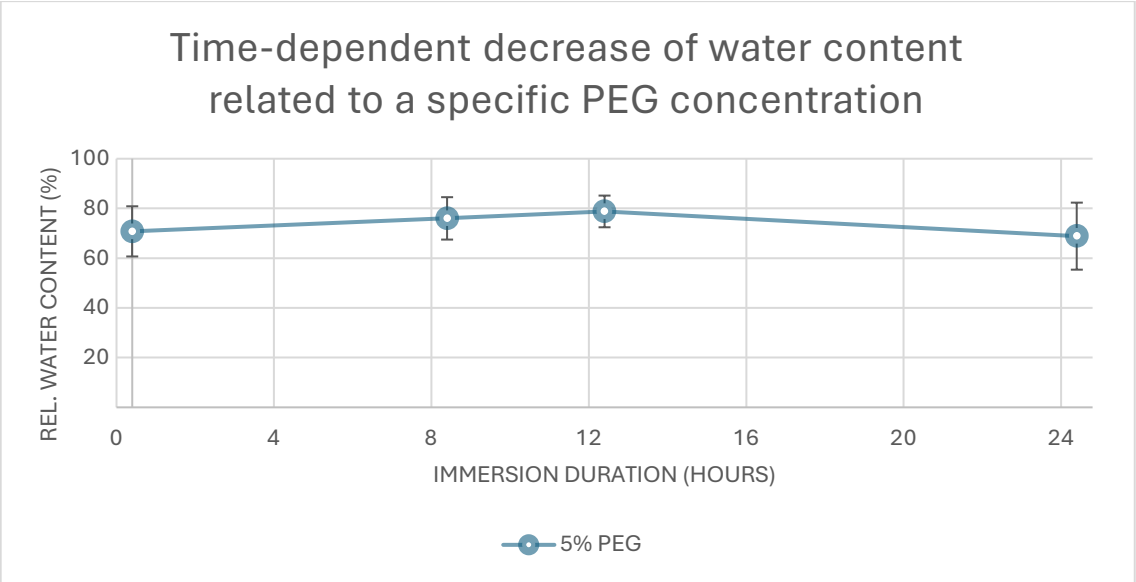

Figure 6: 5% PEG (polyethylene glycol) time-dependent relative water content

		0h	8h	12h	24h
Relative water content [%]	Median	73.46	79.98	80.69	73.77
	Mean	70.78	76.01	78.80	68,86
	Standard deviation	10.09	8.52	6.38	13.48

Table 3: 5% PEG (polyethylene glycol) time-dependent relative water content

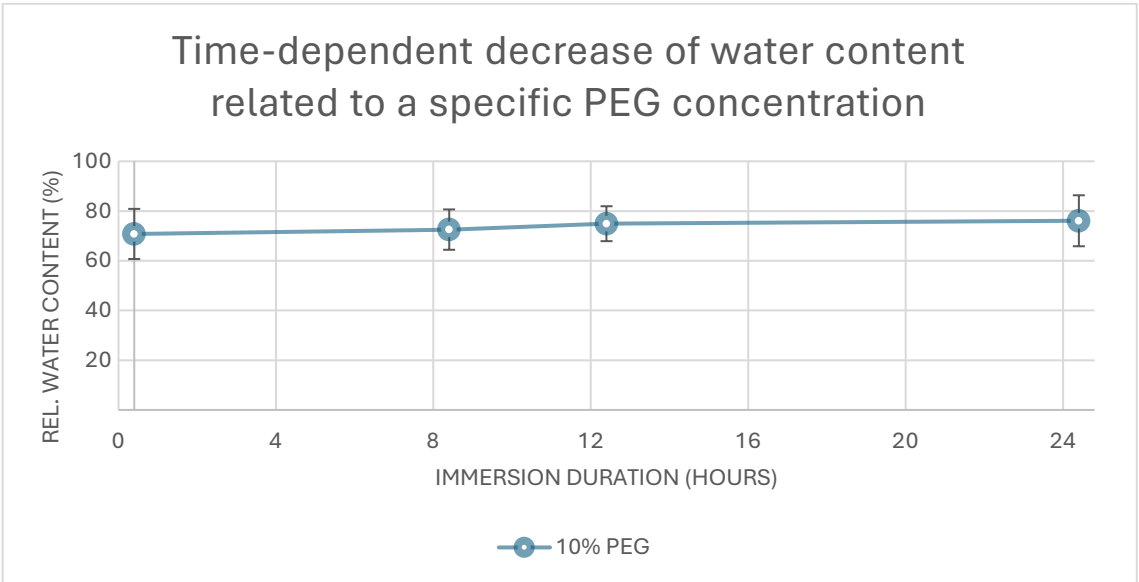

Figure 7: 10% PEG (polyethylene glycol) time-dependent relative water content

		0h	8h	12h	24h
Relative water content [%]	Median	73.46	73.27	77.60	76.92
	Mean	70.78	72.53	74.91	76.08
	Standard deviation	10.09	9.93	5.97	5.99

Table 4: 10% PEG (polyethylene glycol) time-dependent relative water content

2.4 Biomechanical testing group

A total of 35 mucosa samples from three different intraoral sites (hard palate, attached gingiva, free oral mucosa) were harvested from 11 different fresh frozen body donors at the Division of Macroscopic and Clinical Anatomy, Medical University of Graz. The age at the time of death ranged between 70 and 91. 7 were female, 4 were male and they had an edentulous or partially dentate maxilla (1).

2.4.1 Adjusting mucosa water content using the osmotic stress protocol

First, the water content of the tissue samples had to be adjusted to its native value (39). Following the protocol set by the osmotic stress group, the osmotic stress technique was employed to adjust the water content to 71 wt% in all mucosa samples used in the mechanical testing group (39). As shown in Figure 6 and Table 3, the closest value to the native value was obtained using the osmotic stress technique in samples immersed in 5 wt% PEG for 24 hours. For this purpose, the mucosa samples were each packed into a dialysis membrane and sealed on both ends using clamps (39). The clamps were labeled with the respective sample number. The sealed dialysis membranes were then put into containers containing a 5% PEG solution. These containers were then put into a fridge at 4°C under continuous stirring for 24 hours.

Figure 8: Palatal mucosa samples L85 and L43 in dialysis membranes

2.4.2 Mechanical testing

Prior to the mechanical tensile test, dumbbell-shaped specimens were cut from the mucosa samples. This was made possible by 3D-printed blocks in dumbbell-shape measuring 6 mm x 2 mm, into which blades (Tondeo, TSS3, United Salon Technologies GmbH, Solingen) were clamped. The remaining excess tissue was removed using a scalpel.

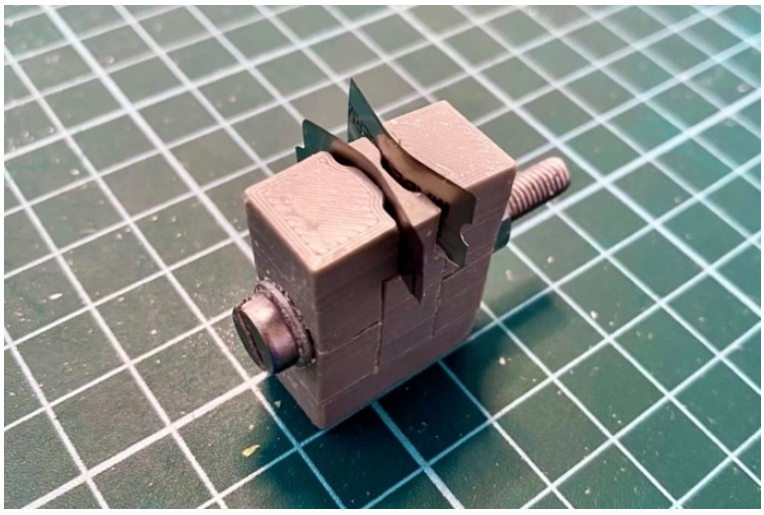

Figure 9: 3D printed dumbbell-shaped mold

The aim was to create dumbbell-shaped tissue samples of the attached gingiva, lining mucosa and hard palate in two different orientations, which are perpendicular to each other. The orientations in the samples of the hard palate were labeled as sagittal (s) and sinister-dexter (sd), while the orientations of the attached gingiva and lining mucosa were labeled bucco-palatal (bp) and along the maxillary crest (kk; Kieferkamm (maxillary crest; mc). The location was marked as “p” for palatal and “v” for vestibular (which includes the attached

gingiva as well as lining mucosa). Tissue supernatants from the dumbbell molds were labeled and frozen at -80°C for histological examination in future studies.

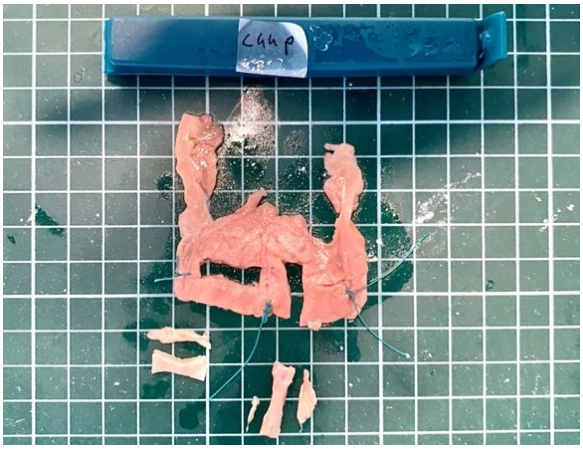

Figure 10: Palatal dumbbell-shaped tissue samples in the orientation "s" and "sd"

Figure 11: Dumbbell-shaped tissue samples of the attached gingiva and lining mucosa in the orientation "mc" and "bp"

The dumbbell-shaped samples were then clamped in specifically manufactured 3D-printed clamps in order to minimize sample slippage during testing. After being clamped, a vinyl polysiloxane (VPS) impression material (Panasil initial contact light, Kettenbach GmbH & Co. KG, Eschenburg, Germany) was applied to the narrow section of the shape to later determine the reference area with a scanner (1). Once solid, the impression material was removed from the specimen with a smooth scalpel cut.

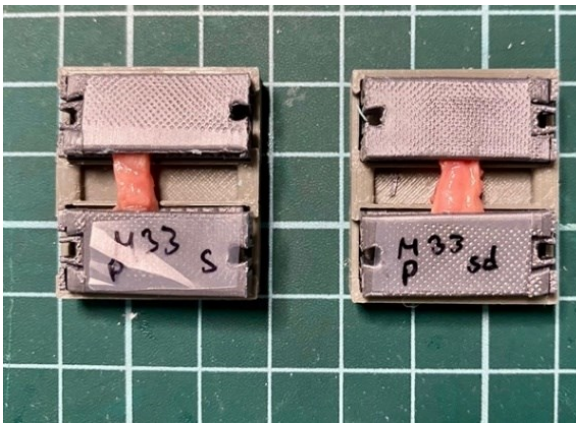

Figure 12: Palatal samples M33 in 3D-printed clamps

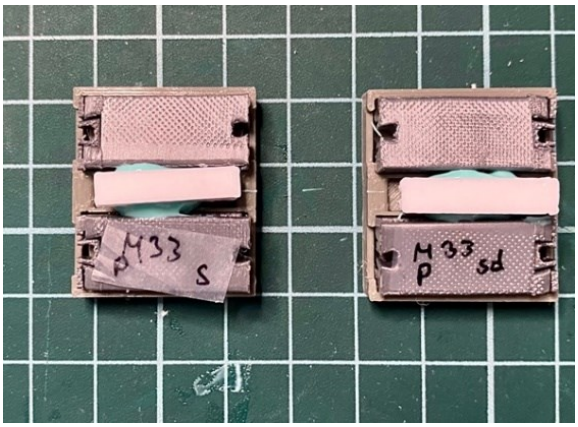

Figure 13: Impression-material on palatal samples M33

Then markers were placed onto the samples for tracking during the tensile test in the later course of the experiment. Once the markers were placed onto the clamped mucosa samples, the samples were clamped into the tensile testing machine (Autograph Shimadzu AGS-10kNG, Shimadzu Corporation, Kyoto, Japan). This electronic, software-controlled (Control

unit: DOLL EDC 60 1278; Software: WinMTPC) testing machine was developed for universal material testing. Thanks to its numerous adjustable parameters, it can be customized to suit specific materials and can generate servo-hydraulic forces of over 1000 N. The samples to be tested can be positioned within a steel frame using two large screw clamps positioned one above the other. This allows a vertical force to be exerted on the test object. The machine is able to collect different, selectable measured variables (force, deflection, etc.), which can be individually defined and measured both digitally and optically (52).

Before starting the uniaxial tensile test, the video extensometer (Videoextensometer ME-46; Operating program: Winext NG, Messphysik Materials Testing GmbH, Fürstenfeld, Austria) was calibrated. The video extensometer provides a high resolution, non-contact strain measurement system, which enables measuring longitudinal and lateral strain. The measurement was performed optically, eliminating the need for physical contact between the extensometer and the test specimen. This method can therefore be applied to all samples without causing slippage or related specimen breakage issues (53). First, the measuring marks had to be determined. As soon as the measuring marks were detected, the tensile test was carried out.

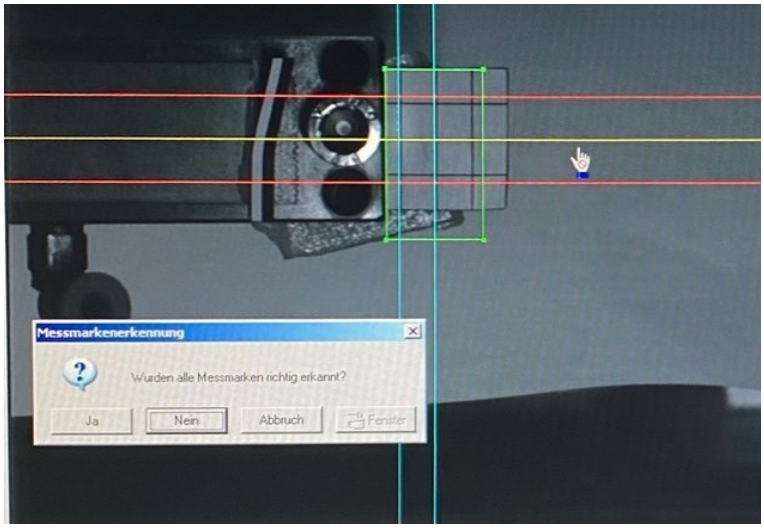

Figure 14: Calibration process of the video extensometer

All uniaxial tensile tests were conducted at a room temperature of 20°C using the same universal testing machine. The gripping length and parallel length of the samples were defined as 6 mm and 3mm, the specimen temperature as 20°C. The standardized direction of the tensile test was defined as straight. Before testing to failure, each sample underwent

20 preconditioning load-unload cycles within a force range of 0.5-2.0 N. The cross-head displacement rate was set at 20 mm/min, for the load-displacement readings a sampling rate of 10 Hz was used (1).

Figure 15: Sample clamped into the uniaxial testing machine

Figure 16: Sample torn by the tensile test, clamped in the uniaxial testing machine

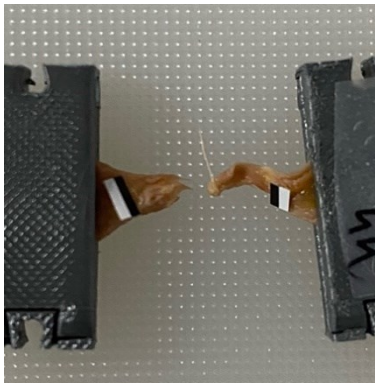

Figure 17: Sample torn by the ultimate tensile test

The torn samples were then labeled and re-frozen at -80°C for future histological examinations.

2.4.3 Scanning

After the impression material was removed from the specimen, it was cut creating a smooth surface, thereby enabling the scan of the cross sections. A commercial scanner (CanoScan LiDE 400, Canon Austria GmbH, Vienna, Austria) with a 600-dpi resolution was utilized to scan the casts of the cross-sections using the Canon IJ Scan Utility software, the cross-sections were analyzed using the Fiji ImageJ_win64 program (1).

Figure 18: Scan of the molds of samples L44 and L92

2.5 Statistical analysis and processing of data

The statistical analysis was performed using MATLAB and Statistics Toolbox (2012b, The MathWorks, Inc., Natick, Massachusetts, United States). Normality of distribution was evaluated using the Shapiro-Wilk test. The ANOVA test was used to compare the differences between the elastic modulus, failure Cauchy stress, failure load and failure stress of the samples harvested from the three regions, with each being tested at right angles to each other. Additionally, ANOVA testing was used to compare the cross-sectional areas of the samples. Post hoc tests were then performed to make multiple comparisons between sample groups, with significance set at 5% ($p \leq 0.05$) (1).

3 Results

Comparison of the anthropometric data of the body donors showed no significant differences in age, height and weight between the specimens used for the osmotic stress protocol and the biomechanical tests (39).

3.1 Osmotic stress protocol

The native samples had an average water content of 71 ± 11 wt%. Immersion in a PEG concentration for 24h resulted in a mean water content of 75.20 ± 10.26 (2.5% PEG), 68.86 ± 13.48 (5% PEG) and 76.08 ± 5.99 (10% PEG), as shown in Table 5. The osmotic stress protocol showed that there was no statistically significant difference in the water content of the specimen when being immersed in 2.5 wt%, 5 wt% or 10 wt% PEG solutions for 24 hours, as the p-value was 0.303. The comparison can be seen in Figure 19. However, studies conducted simultaneously at the Division of Macroscopic and Clinical Anatomy (Medical University of Graz) on the mucosa of the mandible region suggested that the submersion in 5 wt% PEG allows adjusting the water content of the mucosa samples to the initial value (39, 54). The samples were therefore dialyzed in 5 wt% PEG concentration for 24 hours prior to material testing (39).

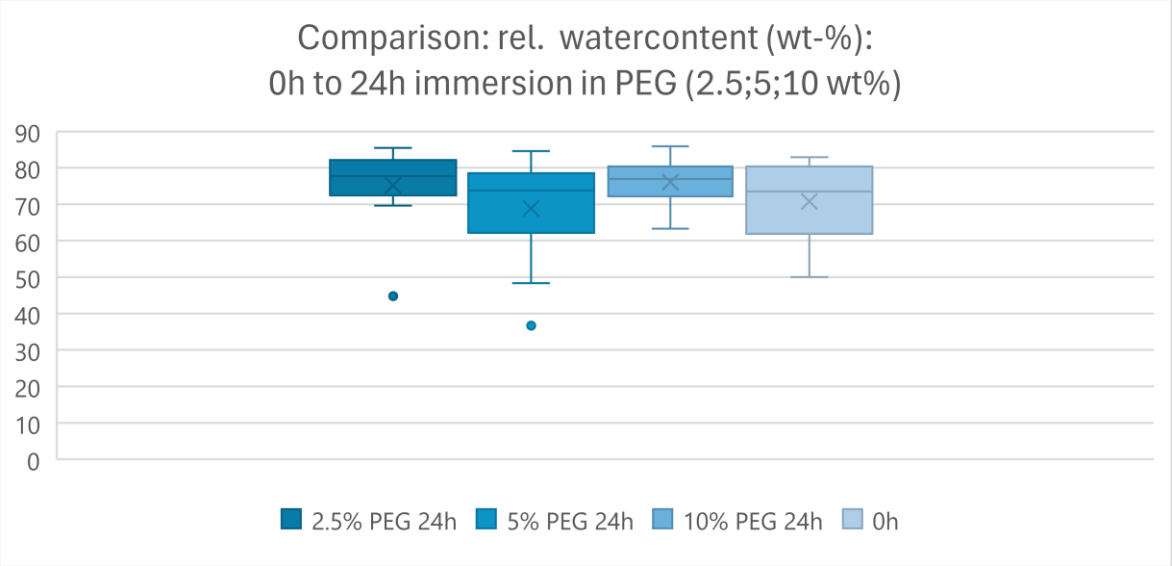

Figure 19: Comparison of 0h samples to samples submersed in 2.5%,5% and 10% PEG (polyethylene glycol) solutions for 24h

		0h (native)	2.5% PEG	5% PEG	10% PEG
Relative water content [%]	Mean	73.46	75.20	68.86	76.08
	Standard deviation	10.09	10.26	13.48	5.99

Table 5: Overview of mean and standard deviation (ordinary one-way ANOVA) of the wt% of the native samples, as well as samples submersed in 2.5%, 5% and 10% PEG (polyethylene glycol) solutions for 24h

3.2 Biomechanical testing

3.2.1 Elastic modulus

Figure 20 shows the elastic modulus of each sample using the regression method. The red tangents in the graph represent the elastic modulus for each sample during the ultimate tensile test. These tangents indicate the stiffness of each sample, reflecting how much they deform under stress. The slope of these tangents corresponds to the elastic modulus, providing insight into the mechanical properties of the tissues tested.

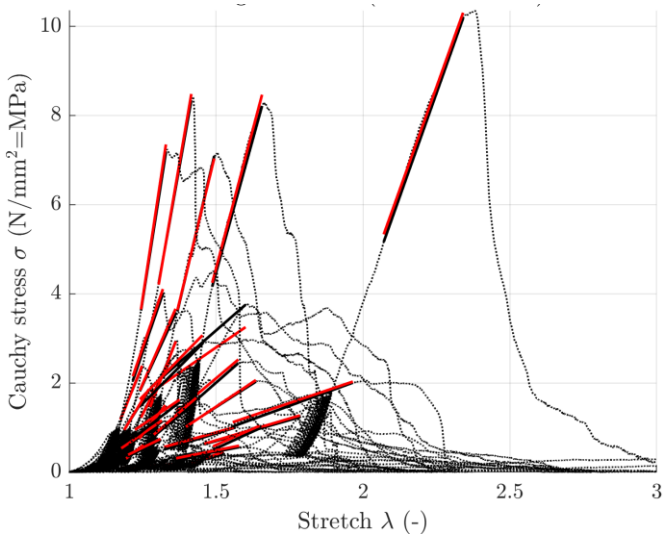

Figure 20: Elastic modulus (MPa) of all samples: regression method

3.2.1.1 Region dependency

The samples' elastic modulus was determined using the linear regression method. The attached gingiva group exhibited the highest mean elastic modulus at 21.3 ± 13.7 MPa, followed by the hard palate samples at 7.9 ± 5.1 MPa, and the buccal mucosa samples at 6.2 ± 4.3 MPa, as detailed in Figure 21 and Table 6. The mean elastic modulus of the attached gingiva was significantly different from the mean elastic modulus of the buccal mucosa

(p=0.049). However, no significant difference was found between the buccal mucosa and hard palate groups (p >0.999) as well as the attached gingiva and hard palate (p=0.134).

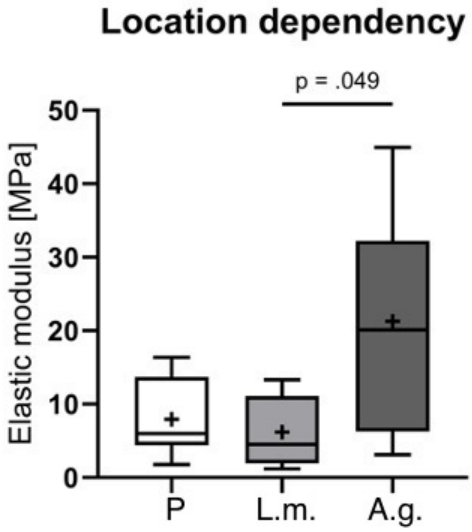

Figure 21: Elastic modulus of the three regions (MPa)

		Palatal (P)	Lining mucosa (L.m.)	Attached ginigiva (A.g.)
Elastic Modulus [MPa]	Mean	7.9	6.2	21.3
	Standard deviation	5.1	4.3	13.7

Table 6: Mean and standard deviations of elastic modulus (MPa); region dependency

3.2.1.2 Direction dependency

In terms of direction dependency, there was no statistically relevant difference found within a region (palate: p=0.699; lining mucosa: p=0.381; attached gingiva: p=0.413) The mean elastic modulus ranged from 2.58 ± 0.65 MPa (lining mucosa: bp) to 25.16 ± 14.83 MPa (attached gingiva: bp). Further details can be seen in Figure 22 and Table 7.

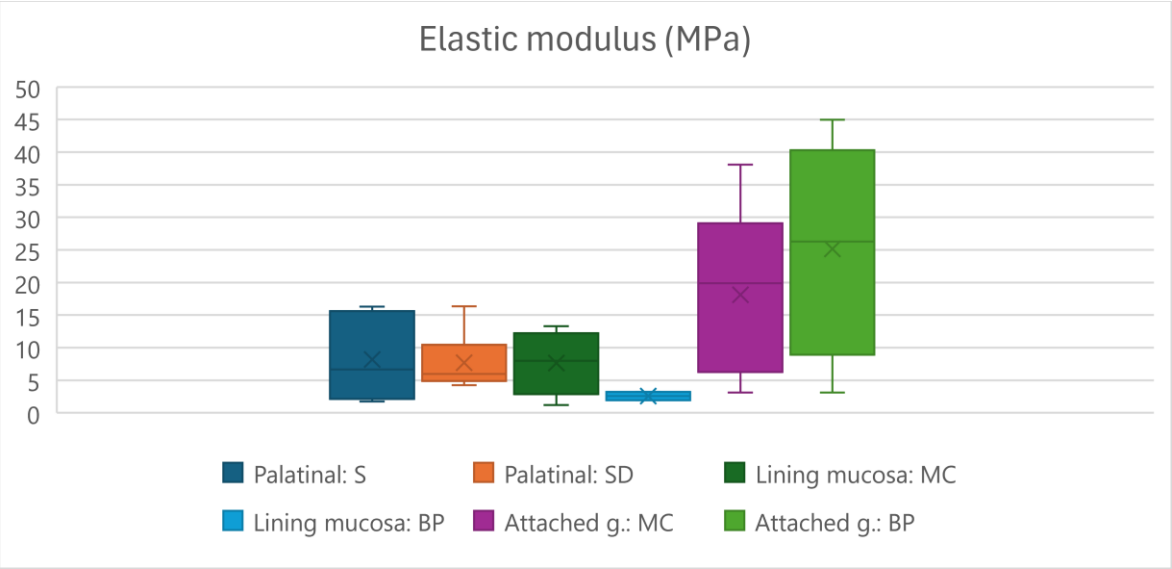

Figure 22: Elastic modulus (MPa) of all sample groups

	P;S	P; SD	L.m.; MC	L.m.; BP	A.g.; MC	A.g.; BP
Mean	8.18	7.68	7.62	2.58	18.13	25.16
Stand. d.	5.84	4.11	4.37	0.65	11.89	14.83

Table 7: Elastic modulus (MPa): Mean and standard deviation (stand. d.) of all sample groups

3.2.2 Failure Cauchy stress

Figure 23 illustrates the stretch on the x-axis and the Cauchy stress (MPa) on the y-axis regarding the ultimate tensile test of each sample. The red markers on the graph indicate the failure Cauchy stress (MPa) for each sample. These markers help identify the point at which each sample reaches its maximum stress before failure. Figures 24-29 show the Cauchy stress of each sample, sorted by region and direction of the sample groups.

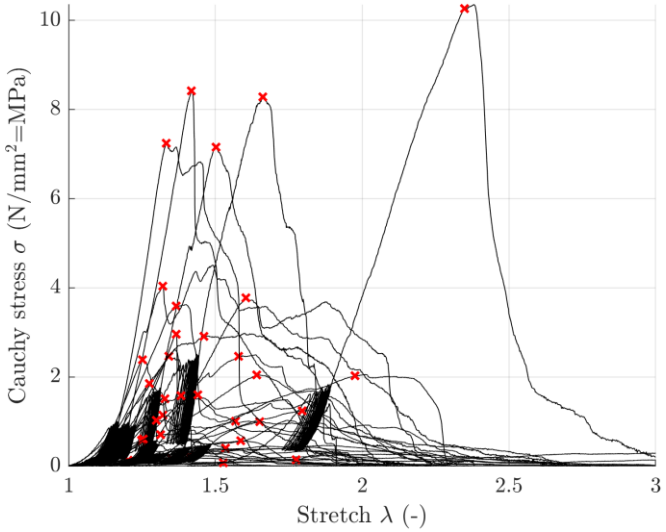

Figure 23: Failure Cauchy stress (MPa) of all samples

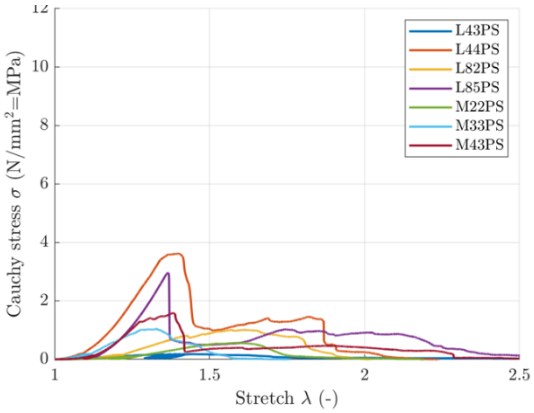

Figure 24: Failure Cauchy stress: Palatal, S

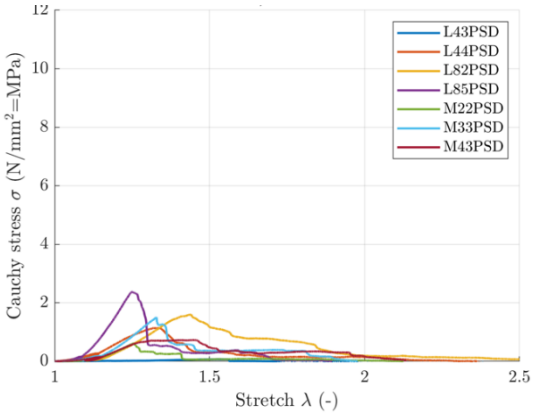

Figure 25: Failure Cauchy stress: Palatal, SD

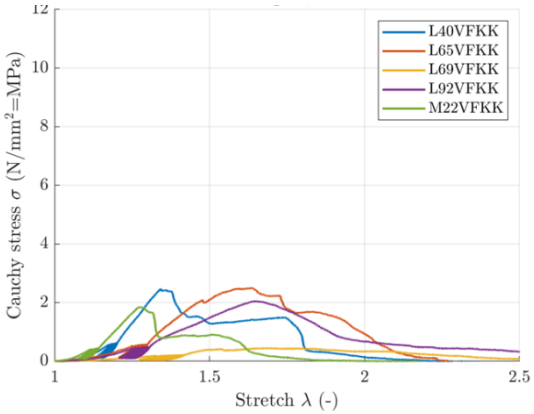

Figure 26: Failure Cauchy stress: Lining mucosa: MC

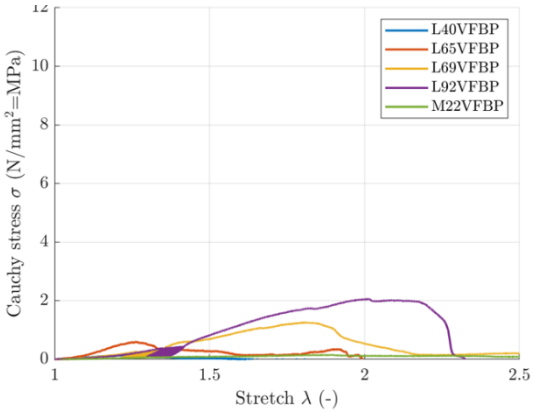

Figure 27: Failure Cauchy stress: Lining mucosa: BP

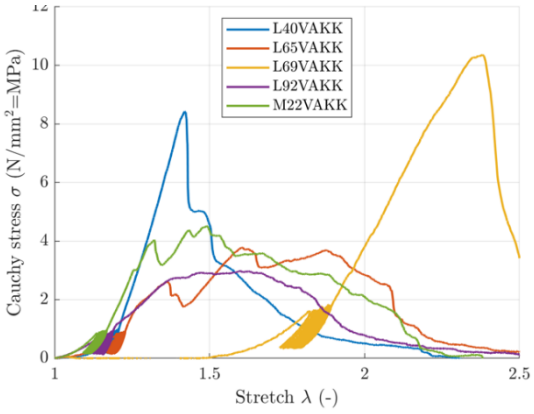

Figure 28: Failure Cauchy stress: Attached gingiva.: MC

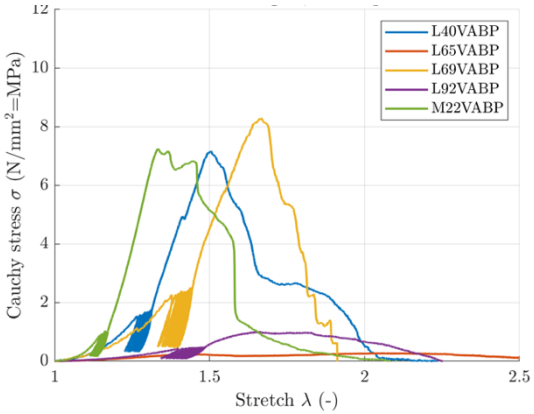

Figure 29: Failure Cauchy stress: Attached gingiva: BP

3.2.2.1 Cross-sectional area

As the failure Cauchy stress is calculated using the samples' cross-sectional area, calculating this parameter was essential (55). By using the Fiji ImageJ_win64 program, the scans of the cross-section casts were analyzed. The cross sections ranged from 2.78 ± 0.25mm² (attached

gingiva, mc) to 17.0 ± 4.26 mm² (palate, s). The palate's cross-sections statistically differed from those of the lining mucosa (p=0.01) and attached gingiva (p<0.001), as seen in Figure 30 and Table 8. There was neither a statistically relevant difference found between the regions lining mucosa and attached gingiva, nor a direction dependency within any of the three regions, as shown in Figure 30 and Figure 31.

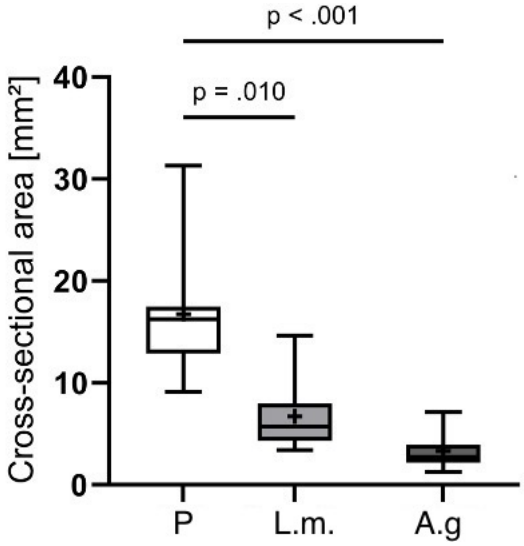

Figure 30: Cross sectional area: location dependency

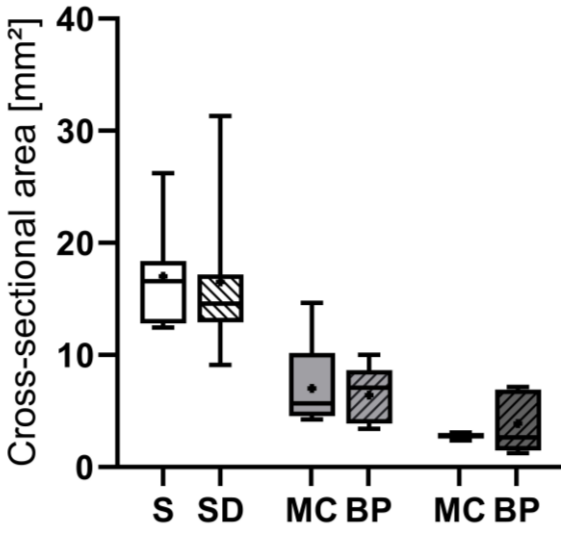

Figure 31: Cross sectional area: direction dependency

		Palatal (P)	Lining mucosa (L.m.)	Attached ginigiva (A.g.)
Cross-sectional area [mm²]	Mean	16.76	6.73	3.33
	Standard deviation	5.53	3.20	1.87

Table 8: Mean and standard deviation of the cross-sectional area (mm²) of the regions palatal, lining mucosa, attached gingiva

3.2.2.2 Region dependency

The attached gingiva group exhibited the highest mean failure Cauchy stress at 5.33 ± 3.23 MPa, followed by the hard palate samples at 1.35 ± 0.99 MPa, and the buccal mucosa samples at 1.33 ± 0.9 MPa, as detailed in Figure 32 and Table 9. The mean failure Cauchy stress of the attached gingiva was significantly different from the mean failure Cauchy stress of the buccal mucosa (p<0.001) and the hard palate (p<0.001). However, no statistically significant difference was found between the buccal mucosa and hard palate (p>0.999).

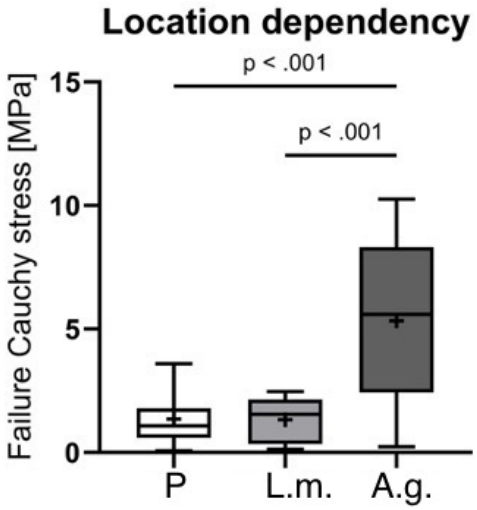

Figure 32: Failure Cauchy stress of the three regions (MPa)

		Palatal (P)	Lining mucosa (L.m.)	Attached ginigiva (A.g.)
Failure Cauchy stress [MPa]	Mean	1.35	1.33	5.33
	Standard deviation	0.99	0.90	3.23

Table 9: Failure Cauchy stress (MPa) of the three regions: mean and standard deviation

3.2.2.3 Direction dependency

In terms of direction dependency, there was no statistically relevant difference found within a region (palate: p=0.469; lining mucosa: p=0.188; attached gingiva: p=0.438). The mean failure Cauchy stress ranged from 0.82 ± 0.72 MPa (lining mucosa: bp) to 5.88 ± 2.91 MPa (attached gingiva: mc), as shown in Figure 33 and Table 10.

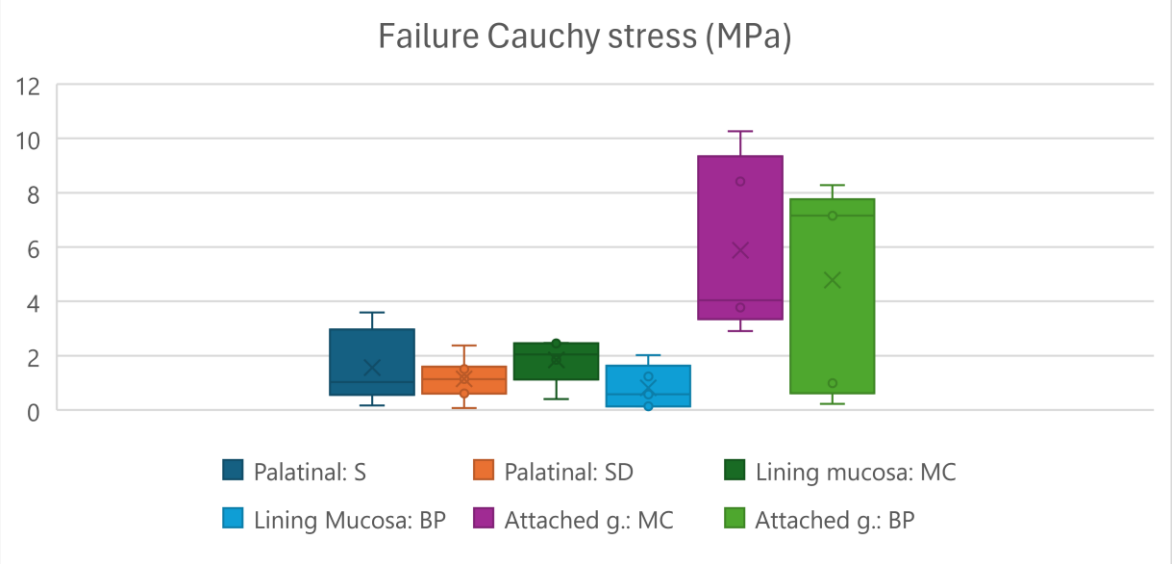

Figure 33: Failure Cauchy stress (MPa) of all sample groups

	P;S	P; SD	L.m.; MC	L.m.; BP	A.g.; MC	A.g.; BP
Mean	1.56	1.15	1.84	0.82	5.88	4.78
Stand. d.	1.17	0.71	0.76	0.72	2.91	3.43

Table 10: Failure Cauchy stress (MPa): Mean and standard deviation of all sample groups

3.2.3 Failure load

Figure 34 displays the force F (N) applied at maximum stretch during the ultimate tensile test, just before the tissue samples ruptured. The maximum load (N) of each sample is marked with a red "x" on the graph. The maximum load represents the highest amount of force each sample could withstand before breaking, indicating the tensile strength of the tissue.

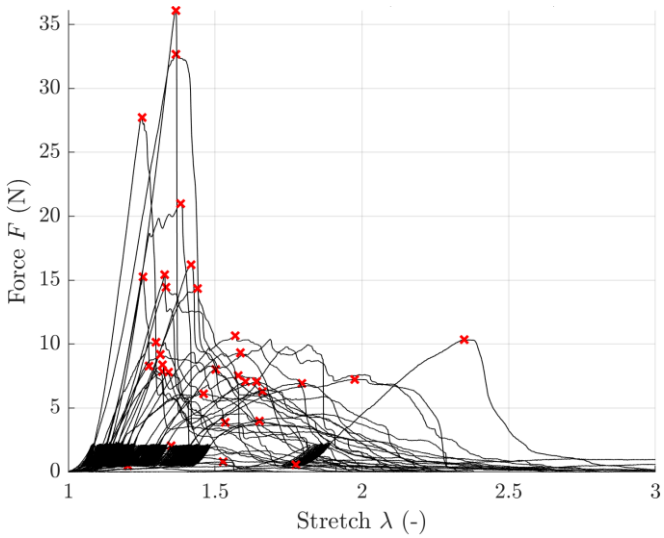

Figure 34: Failure load (N) of all samples: load vs stretch

3.2.3.1 Region dependency

The palatal group exhibited the highest mean failure load at 15.18 ± 10.30 N, followed by the attached gingiva samples at 8.21 ± 4.29 N, and the buccal mucosa samples at 5.14 ± 3.02 N, as detailed in Table 11. The mean failure load of the hard palate was significantly different from the mean failure load of the buccal mucosa (p=0.004), as detailed in Figure 35. There was neither a statistically significant difference found between the buccal mucosa and attached gingiva (p=0.534), nor the hard palate and the attached gingiva (p=0.227).

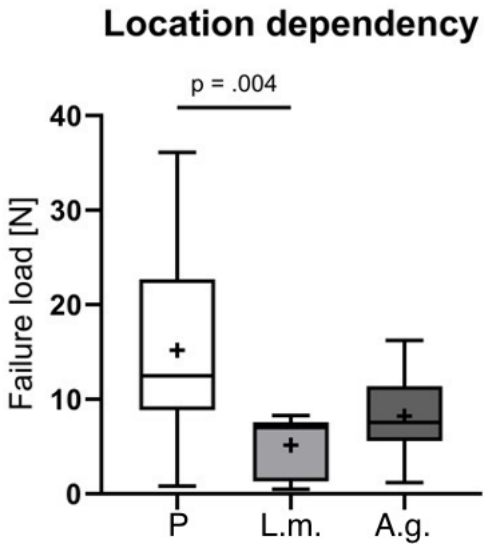

Figure 35: Failure load of the three regions (N)

		Palatal (P)	Lining mucosa (L.m.)	Attached ginigiva (A.g.)
Failure load [MPa]	Mean	15.18	5.14	8.21
	Standard deviation	10.30	3.02	4.29

Table 11: Failure load (N) of the three regions: mean and standard deviation

3.2.3.2 Direction dependency

In terms of direction dependency, there was no statistically relevant difference found within a region (hard palate: p=0.469; lining mucosa: p=0.312; attached gingiva: p=0.438). The mean elastic modulus ranged from 3.36 ± 3.07 MPa (lining mucosa: bp) to 17.42 ± 11.93 MPa (hard palate: s) as detailed in Figure 36 and Table 12.

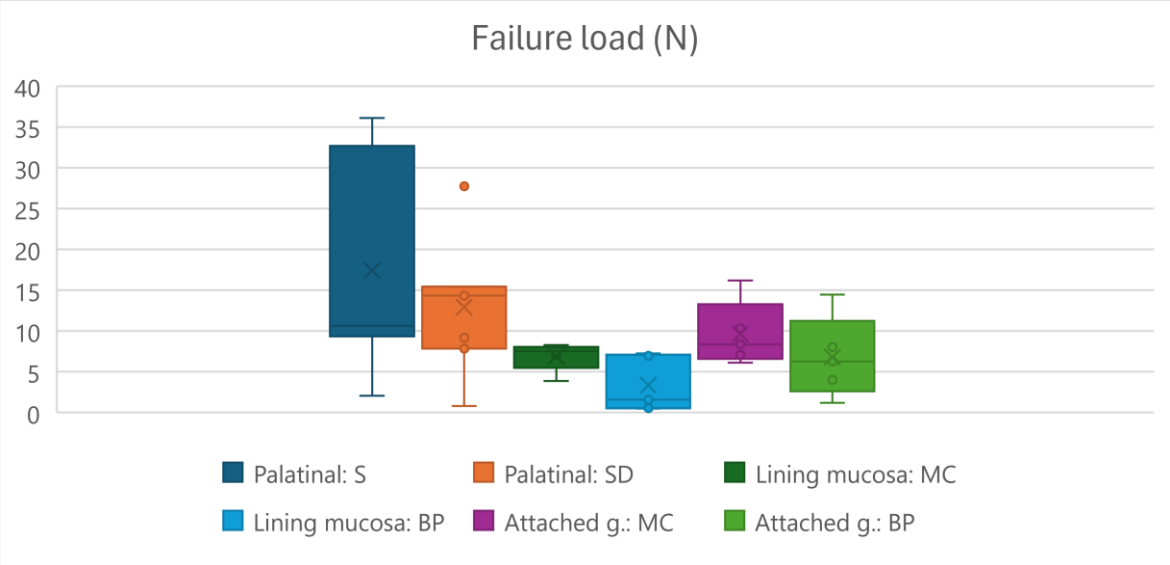

Figure 36: Failure load (N) of all sample groups

	P;S	P; SD	L.m.; MC	L.m.; BP	A.g.; MC	A.g.; BP
Mean	17.42	12.94	6.91	3.36	9.62	6.78
Stand. d.	11.93	7.74	1.57	3.07	3.58	4.47

Table 12: Failure load (N): Mean and standard deviation of all sample groups

3.2.4 Failure stretch

Figure 37 displays the failure stretch on the x-axis and the force F (N) on the y-axis. The red markers indicate the failure stretch in the ultimate tensile test for each tissue sample. The failure stretch of a tissue represents the amount of deformation or elongation the tissue undergoes before reaching its breaking point under applied force (28). This parameter is crucial for understanding the mechanical properties and resilience of different tissue types.

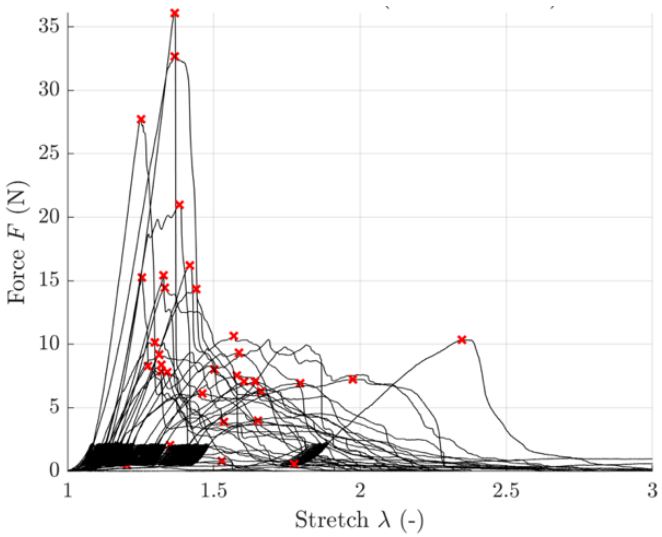

Figure 37: Failure stretch of all samples: load vs stretch

3.2.4.1 Region dependency

The failure stretches of the three regions ranged from 1.38 ± 0.10 in the hard palate, to 1.54 ± 0.25 in the lining mucosa and 1.57 ± 0.25 in the attached gingiva, as shown in Table 13. There was no statistically relevant difference found between the regions (pal. vs. lining mucosa: p=0.469; pal. vs. attached g.: p=0.137; lining mucosa vs attached gingiva: p>0.999), as demonstrated in Figure 38.

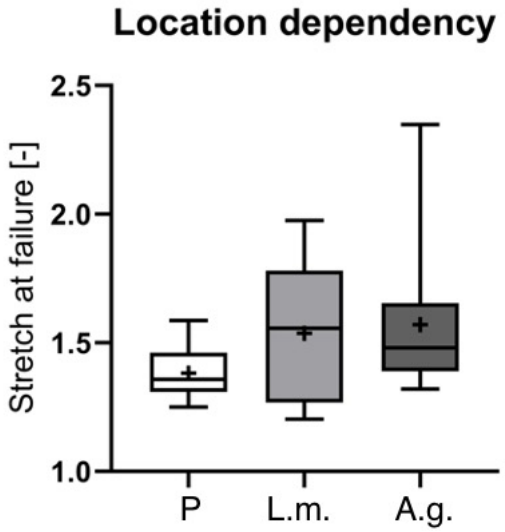

Figure 38: Failure stretch of the three regions

		Palatal (P)	Lining mucosa (L.m.)	Attached ginigiva (A.g.)
Failure stretch	Mean	1.38	1.54	1.57
	Standard deviation	0.10	0.25	0.28

Table 13: Failure stretch of the three regions: mean and standard deviation

3.2.4.2 Direction dependency

No statistically relevant difference was found within a region in terms of directional dependency (hard palate: p=0.297; buccal mucosa: p=0.438; attached gingiva: p=0.812). The mean failure stretch ranged from 1.35 ± 0.09 (hard palate: sd) to 1.63 ± 0.37 (attached gingiva: mc) as shown in Figure 39 and Table 14.

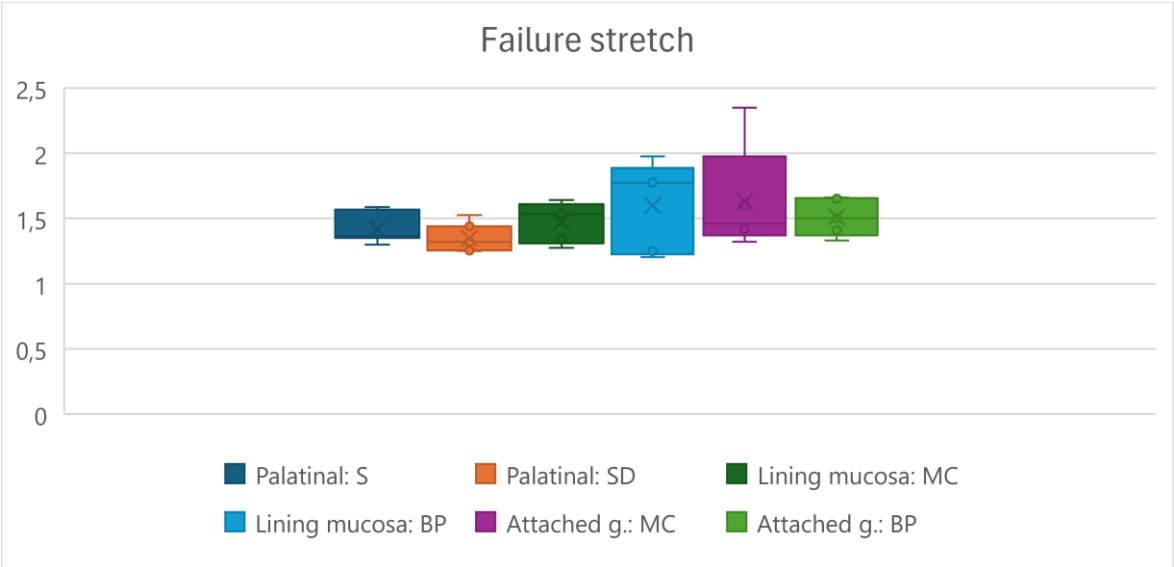

Figure 39: Failure stretch of all sample groups

	P;S	P; SD	L.m.; MC	L.m.; BP	A.g.; MC	A.g.; BP
Mean	1.42	1.35	1.47	1.60	1.63	1.51
Stand. d.	0.10	0.09	0.14	0.31	0.37	0.13

Table 14: Failure stretch: Mean and standard deviation of all sample groups

4 Discussion

This study is the first to investigate fresh-frozen tissues of the human oral mucosa of the maxilla region, allowing direct comparisons between tissues from three different intraoral regions (hard palate, lining mucosa, attached gingiva) and additionally takes directional dependence into account. The primary hypothesis, which proposed a difference in the modulus of elasticity, failure Cauchy stress as well as failure load and failure stretch of oral mucosa tissues from three different intraoral sites from the maxillary region, was confirmed. The study's findings indicate that mucosa tissues from different intraoral regions exhibit different mechanical behaviors. The second hypothesis, which indicated a directional dependence regarding the mechanical characteristics within the three regions was rejected, as the study's findings did not reveal directional dependence within a region for any of the mechanical parameters tested.

4.1 Osmotic stress protocol: Results and comparison with previous studies

There were no statistically significant differences in the results of the 3 different PEG concentrations (2.5 wt%, 5 wt%, 10 wt%) with respect to the osmotic stress protocol. However, in order to match the samples as closely as possible to native conditions, the results of a parallel study on the mandibular mucosa were used: this study showed that the mandibular mucosa was best matched to native conditions when immersed for 24 hours at a PEG concentration of 5 wt% (54). The results of neither the concurrent study nor this study followed a time-dependent exponential function as suggested by previous studies. In the concurrent study of mandibular mucosa, there was an increase in water content in the samples after 8 hours in 2.5 wt% and 5 wt% PEG concentrations, but this was followed by a decrease, showing the expected dehydration. The samples immersed in a 10 wt% PEG solution showed an increase in tissue water content, which is unusual as PEG solutions should dehydrate the tissue by osmosis (39, 54). In this study, the water content of the tissues showed an increase within the first 12 hours of immersion in 2.5 wt%, 5 wt% and 10 wt% PEG concentrations. Following the increase, a decrease was observed between 12 and 24 hours of immersion in 2.5 wt% and 5 wt% PEG concentrations, following the expected dehydration. No dehydration was observed in the samples immersed in 10 wt% PEG concentrations for 24 hours.

Previous studies have demonstrated that when tissues are exposed to different concentrations of PEG for 24 hours, the water content of these tissues decreases exponentially over time: The higher the PEG concentration, the lower the water content in the tissue. However, this study was carried out on fresh-frozen samples of the iliotibial tract, a different type of tissue composition from that of the mucosa (39).

4.2 Mechanical testing group: Results and comparison with previous studies

In this study, the attached gingiva had the highest modulus of elasticity, followed by the hard palate and the buccal mucosa. These results are corresponding to the previous studies that used the Thiel-embalmed oral mucosa (1). However, this study yielded a statistically significant difference between the attached gingiva and the buccal mucosa, whereas previous studies also found a significant difference in the modulus of elasticity between the attached gingiva and the hard palate (1).

The region dependent failure Cauchy stress, which was also called 'tensile stress' in other studies, was highest in the attached gingiva samples in this study. There was a statistically significant difference between the attached gingiva and the other two regions, but not between the hard palate and the buccal mucosa. These findings are in line with a previous study (1).

Regarding the failure load (N) in the ultimate tensile test, there are currently no studies on the behavior of oral mucosa in different regions using human tissue samples. However, studies have investigated the failure load in the regions of attached gingiva and buccal mucosa using porcine tissue. These findings, similar to the results of this study, suggest that the failure load is higher in the attached gingiva region than in the buccal mucosa (56).

As histological examinations were not performed in this study, the reasons for the behavior of tissues from different regions can only be speculated. Previous research suggests that attached gingiva tissues have predominantly unidirectional collagen fiber networks and unraveled elastin, in contrast to the hard palate and lining mucosa. Tissues from the hard palate region showed denser fibers and reticular tissue in random directions. Compared to the attached gingiva, collagen fibers in the hard palate were denser but less oriented. Buccal

mucosal tissues showed thinner bundles of fibers arranged in multiple directions (1). However, these histological findings from other studies need to be validated for the tissue samples used in this study by performing an additional histological examination on them.

4.3 Limitations

There were several potential influencing factors in this study that should be acknowledged. Firstly, the sample size was relatively small, as tissue samples were obtained from only 11 body donors (7 female, 4 male). This limited study population may not be fully representative and could affect the generalizability of the results.

Additionally, the duration for which the fresh-frozen body donors were stored prior to tissue removal is unknown. The length of time the donors remained frozen could have several effects on the tissue properties, introducing variability that we were unable to account for. Moreover, it is also unclear whether the samples were unintentionally thawed during handling and preparation. Thawing and refreezing cycles can significantly alter tissue characteristics, potentially compromising the integrity of the samples.

Moreover, there is also a lack of detailed records regarding the storage conditions of the samples. Ideally, the tissue samples should have been stored consistently at -80°C. However, any deviation from this optimal storage temperature, whether due to equipment malfunction or other issues, could have affected the quality and mechanical properties of the tissues. Prolonged storage at -80°C could potentially impact or destroy cells within the tissues, adding another layer of uncertainty to our findings. Without precise monitoring and documentation of the storage conditions, it is difficult to exclude temperature fluctuations as a source of variability in the results.

Furthermore, without histological examination of the samples, we cannot fully explain the observed mechanical results. Histological analysis would provide insight into the cellular and structural integrity of the tissues and help to elucidate the underlying reasons for their mechanical behavior.

Future research should aim to include a larger sample size, ensure strict adherence to controlled storage conditions and include thorough histological examinations to validate and extend the findings of this study.

There are several limitations to consider regarding the results of the osmotic stress protocol. Firstly, histological evaluation is crucial for a thorough understanding of the findings. Cell damage may have occurred due to shock freezing or prolonged storage at -80°C, resulting in an inadequate number of intact cells for the osmotic stress protocol. Furthermore, the container in which the filled dialysis membranes were immersed may have been too small, or the solution volume may have been insufficient for the amount of tissue samples tested. A comprehensive histological analysis will help to identify and address these potential issues, ensuring the reliability of the experimental results.

4.4 Clinical implications

Understanding how the mucosa responds biomechanically to dental restorations is essential in order to improve treatment outcomes and minimize patient discomfort. By studying the mechanical properties of oral mucosa and tissue structures, we can advance the development of better synthetic materials and structures. This knowledge is essential for improving denture foundations in both fully and partially edentulous patients, allowing better management of traumatized tissues and providing patients with clear guidelines for tissue recovery after occlusal loading. In addition, it is important to identify areas where the use of prophylactic denture liners can protect tissues with lower tensile strength. Quantitative mechanical analysis of human oral tissues is essential for advancing both material development and clinical practice to ensure that new materials effectively mimic natural tissue behavior (1, 4).

4.5 Conclusion and future perspectives

The findings demonstrate that the attached gingiva is stiffer and has a higher failure Cauchy stress compared to the hard palate and buccal mucosa. To properly verify the results regarding the locational dependency of the maxillary oral mucosa and reassess the directional dependency of the tissues' mechanical properties within a region, a future comprehensive histological examination is essential. This should include a detailed analysis of the different cell types present, the composition and structure of the fibers, and the

orientation of these fibers within the tissue. By thoroughly studying these histological aspects, we can gain an understanding of the factors that influence the mechanical behavior of the oral mucosa and ensure the accuracy and reliability of our findings. Such detailed histological insights are crucial to validate the conclusions of our study and could potentially reveal nuances in tissue behavior that could not be detected by mechanical testing alone.

References

1. Choi JJE, Zwirner J, Ramani RS, Ma S, Hussaini HM, Waddell JN, et al. Mechanical properties of human oral mucosa tissues are site dependent: A combined biomechanical, histological and ultrastructural approach. Clin Exp Dent Res. 2020;6(6):602-11.
2. Atlas AM, Behrooz E, Barzilay I. Can bite-force measurement play a role in dental treatment planning, clinical trials, and survival outcomes? A literature review and clinical recommendations. Quintessence Int. 2022;53(7):632-42.
3. Basker RMD, J. C. Prosthetic Treatment of the Edentulous Patient. Fourth Edition ed: Blackwell; 2002.
4. Chen J, Ahmad R, Li W, Swain M, Li Q. Biomechanics of oral mucosa. J R Soc Interface. 2015;12(109):20150325.
5. Oral Cavity and Nasopharyngeal Cancers Screening (PDQ(R)): Patient Version. PDQ Cancer Information Summaries. Bethesda (MD)2002.
6. Schünke MS, Erik; Schumacher, Udo. Prometheus LernAtlas der Anatomie: Kopf, Hals und Neuroanatomie. Stuttgart: Thieme; 2018.
7. Waschke JP, Friedrich. Sobotta, Atlas der Anatomie des Menschen Band 3: Urban & Fischer in Elsevier; 2022.
8. Maio; GAGAACJEJKG. Duale Reihe Anatomie. Stuttgart: Georg Thieme Verlag 2020.
9. Helwany M, Rathee M. Anatomy, Head and Neck, Palate. StatPearls. Treasure Island (FL)2024.
10. Kamrani P, Sadiq NM. Anatomy, Head and Neck, Oral Cavity (Mouth). StatPearls. Treasure Island (FL)2024.
11. Wenz H-J, Hellwig E, editors. Zahnärztliche Propädeutik: Einführung in die Zahnheilkunde 14. A2018; Köln: Deutscher Zahnärzte Verlag.
12. Wolf HF, Rateitschak EM, Rateitschak KH. Parodontologie: Thieme; 2004.
13. Lüllmann-Rauch R, Asan E. Taschenlehrbuch Histologie. 5., vollständig überarbeitete Auflage ed. Stuttgart ; New York: Georg Thieme Verlag; 2015.
14. Shum J, Blanco A, Guo S, Marruffo J, Melville JC. 25 - Early Buccal Mucosa Cancer. In: Bell RB, Fernandes RP, Andersen PE, editors. Oral, Head and Neck Oncology and Reconstructive Surgery: Elsevier; 2018. p. 532-43.
15. Platzer W. Taschenatlas Anatomie. Stuttgart: Georf Thieme Verlag; 2009.
16. Fitzpatrick TH, Downs BW. Anatomy, Head and Neck, Nasopalatine Nerve. StatPearls. Treasure Island (FL)2024.
17. Miller AJ. Oral and pharyngeal reflexes in the mammalian nervous system: their diverse range in complexity and the pivotal role of the tongue. Crit Rev Oral Biol Med. 2002;13(5):409-25.
18. Gängler PH, Thomas; Willershausen, Britta; Schwenzer, Norbert; Ehrenfeld, Michael. Konservierende Zahnheilkunde und Parodontologie. Stuttgart: Georg Thieme Verlag; 2010.
19. Capra NF. Mechanisms of oral sensation. Dysphagia. 1995;10(4):235-47.
20. Brizuela M, Winters R. Histology, Oral Mucosa. StatPearls. Treasure Island (FL)2024.
21. Winning TA, Townsend GC. Oral mucosal embryology and histology. Clin Dermatol. 2000;18(5):499-511.
22. Nanci A. Ten Cate's oral histology : development, structure, and function. St. Louis, Missouri: Elsevier; 2018.

23. Fleisch L, Austin JC. A histologic study of the response of masticatory and lining mucosa to mechanical loading in the vervet monkey. J Prosthet Dent. 1978;39(2):211-6.
24. Adams D. Keratinization of the oral epithelium. Ann R Coll Surg Engl. 1976;58(5):351-8.
25. Kydd WL, Daly CH, Nansen D. Variation in the response to mechanical stress of human soft tissues as related to age. J Prosthet Dent. 1974;32(5):493-500.
26. Winny Yohana JS, Moch Rodian Biomechanical Aspects of the Oral Mucosa in Clinical Implications: Scoping Review
. Journal of International Dental and Medical Research. 2023;16:888-98.
27. Hammer N, Loffler S, Feja C, Sandrock M, Schmidt W, Bechmann I, et al. Ethanol-glycerin fixation with thymol conservation: a potential alternative to formaldehyde and phenol embalming. Anat Sci Educ. 2012;5(4):225-33.
28. Estermann SJ, Forster-Streffleur S, Hirtler L, Streicher J, Pahr DH, Reisinger A. Comparison of Thiel preserved, fresh human, and animal liver tissue in terms of mechanical properties. Ann Anat. 2021;236:151717.
29. Antipova V, Niedermair JF, Siwetz M, Fellner FA, Loffler S, Manhal S, et al. Undergraduate medical student perceptions and learning outcomes related to anatomy training using Thiel- and ethanol-glycerin-embalmed tissues. Anat Sci Educ. 2023;16(6):1144-57.
30. Coleman R, Kogan I. An improved low-formaldehyde embalming fluid to preserve cadavers for anatomy teaching. J Anat. 1998;192 (Pt 3)(Pt 3):443-6.
31. Stouthandel MEJ, Vanhove C, Devriendt W, De Bock S, Debbaut C, Vangestel C, et al. Biomechanical comparison of Thiel embalmed and fresh frozen nerve tissue. Anat Sci Int. 2020;95(3):399-407.
32. Balta JY, Cronin M, Cryan JF, O'Mahony SM. Human preservation techniques in anatomy: A 21st century medical education perspective. Clin Anat. 2015;28(6):725-34.
33. Changoor A, Fereydoonzad L, Yaroshinsky A, Buschmann MD. Effects of refrigeration and freezing on the electromechanical and biomechanical properties of articular cartilage. J Biomech Eng. 2010;132(6):064502.
34. Stemper BD, Yoganandan N, Stineman MR, Gennarelli TA, Baisden JL, Pintar FA. Mechanics of fresh, refrigerated, and frozen arterial tissue. J Surg Res. 2007;139(2):236-42.
35. Hammer N, Loffler S, Bechmann I, Steinke H, Hadrich C, Feja C. Comparison of modified Thiel embalming and ethanol-glycerin fixation in an anatomy environment: Potentials and limitations of two complementary techniques. Anat Sci Educ. 2015;8(1):74-85.
36. McDougall S, Soames R, Felts P. Thiel embalming: Quantifying histological changes in skeletal muscle and tendon and investigating the role of boric acid. Clin Anat. 2020;33(5):696-704.
37. Siess MB. On the potential morpho-mechanical link between the gluteus maximus and pelvic floor tissues: Medical University of Graz; 2023.
38. Gerle FM, Pauline; Boisselet, Christelle; Lafleuriel, David; Godfroy, Julien; Lochin, Pierre; Marteau, Baptiste; Piégay, Hervé; Puijalon, Sara; Vernay, Antoine Intrinsic water use efficiency estimate: an
isotopic method 2023.
39. Hammer N, Huster D, Fritsch S, Hadrich C, Koch H, Schmidt P, et al. Do cells contribute to tendon and ligament biomechanics? PLoS One. 2014;9(8):e105037.

40. Schiffter-Weinle H. PEG - das Multitalent. Deutsche Apotheker Zeitung. 2015;26:38.
41. Hagel V, Haraszti T, Boehm H. Diffusion and interaction in PEG-DA hydrogels. Biointerphases. 2013;8(1):36.
42. Reitemeier B, Biffar R. Einführung in die Zahnmedizin: Thieme; 2006.
43. Harris DC. Quantitative Chemical Analysis. 7 ed: W. H. Freeman and Company; 2007.
44. Laborpraxis Band 4: Analytische Methoden: Springer International Publishing; 2016.
45. Schmidt C, Dietrich L. Chemie für Biologen: Von Studierenden für Studierende erklärt: Springer Berlin Heidelberg; 2014.
46. Schiller LR, Emmett M, Santa Ana CA, Fordtran JS. Osmotic effects of polyethylene glycol. Gastroenterology. 1988;94(4):933-41.
47. Westlab. Westlab. 2023 11.09.2023. [cited 2024 16.04.2024]. Available from: https://www.westlab.com.au/blog/the-role-of-hydrochloric-acid-in-ph-balancing-of-water.
48. KG SLIGC. Quintix® and Secura®
Standard Laboratory Balances: Reliable Weighing for Faster and Better Results. 2022.
49. Adams GD, Cook I, Ward KR. The principles of freeze-drying. Methods Mol Biol. 2015;1257:121-43.
50. Shiguetomi-Medina JM, Ramirez-Gl JL, Stodkilde-Jorgensen H, Moller-Madsen B. Systematized water content calculation in cartilage using T1-mapping MR estimations: design and validation of a mathematical model. J Orthop Traumatol. 2017;18(3):217-20.
51. Bhambere DG, Kunal; Harwalkar, Mallinath; Nirgude, Pallavi. LYOPHILIZATION / FREEZE DRYING – A REVIEW. World Journal of Pharmaceutical Research. 2015.
52. Wallner J. Die Anwendung der Herbert-Knochen-Schraube in der osteosynthetischen Behandlung von Frakturen des Kieferwinkels: Ein biomechanischer Vergleich zur konventionellen Miniplattenosteosynthese. Graz: Medizinische Universität Graz; 2015.
53. Toygar E, Gulakman A. Failure Modes in Fiber Reinforced Composites and Fracture Toughness Testing of FRP. 2022.
54. Radetzky C. Morphological description of the human oral mucosa - Focus on the mechanical properties of the mandibular part. Graz: Medical University of Graz; 2024.
55. Rigelesaiyin J, Diaz A, Li W, Xiong L, Chen Y. Asymmetry of the atomic-level stress tensor in homogeneous and inhomogeneous materials. Proc Math Phys Eng Sci. 2018;474(2217):20180155.
56. Goktas S, Dmytryk JJ, McFetridge PS. Biomechanical behavior of oral soft tissues. J Periodontol. 2011;82(8):1178-86.

Attachment

Sample ID	Ref. area (mm^2)	Failure stretch (-)	Failure load (N)	Failure Cauchy stress (N/mm^2=MPa)	Elastic modulus, regr. method (N/mm^2=MPa)
L43PS	15.94	1.350517989	2.045	0.173262816	0.480386931
L44PS	12.44	1.366550807	32.677	3.589612598	15.04402543
L82PS	16.57	1.568019839	10.645	1.007336825	1.854156924
L85PS	16.65	1.366028302	36.105	2.9621893	16.80460654
M22PS	26.23	1.586918917	9.324	0.564103392	1.311928055
M33PS	12.82	1.298210532	10.145	1.027328069	4.48589515
M43PS	18.38	1.38277651	20.999	1.579810878	4.440628118
L43PSD	17.19	1.526740593	0.805	0.071496578	*
L44PSD	9.1	1.320219884	7.843	1.137855445	4.553278205
L82PSD	12.9	1.439574401	14.333	1.599489914	5.717130717
L85PSD	14.57	1.250855619	27.731	2.380746545	16.51340759
M22PSD	31.33	1.254945162	15.251	0.61088952	5.136723973
M33PSD	13.6	1.328469289	15.427	1.506933509	8.444995279
M43PSD	17	1.312734758	9.179	0.70879955	3.230224597
L40VFKK	4.24	1.341911551	7.795	2.467028429	13.03178454
L65VFKK	4.83	1.578717609	7.521	2.458288848	5.557469539
L69VFKK	14.64	1.534037596	3.881	0.40666666	2.464144139
L92VFKK	5.67	1.641033125	7.07	2.04622649	4.408263527
M22VFKK	5.73	1.275462206	8.294	1.84619259	10.8490644
L40VFBP	4.36	1.203396697	0.483	0.133312065	*
L65VFBP	3.4	1.247928094	1.578	0.579185451	*
L69VFBP	10.03	1.79622366	6.941	1.243029753	1.960236104
L92VFBP	7.07	1.975483949	7.247	2.024940902	2.224874884
M22VFBP	7.29	1.774918157	0.563	0.137075298	*
L40VAKK	2.73	1.418763473	16.201	8.419555686	38.45044961
L65VAKK	3	1.603343132	7.07	3.778545315	4.537974865
L69VAKK	2.37	2.348526947	10.356	10.26217091	18.40071571
L92VAKK	3.07	1.46042687	6.12	2.911339559	6.742527273
M22VAKK	2.74	1.321010809	8.374	4.037279021	19.10965544
L40VABP	1.68	1.501664941	8.004	7.154360826	27.17870784
L65VABP	7.16	1.408708099	1.191	0.234325607	*
L69VABP	1.26	1.661033244	6.281	8.280118891	24.86896514
L92VABP	6.65	1.65143835	3.994	0.991856356	2.903205476
M22VABP	2.66	1.332326284	14.462	7.243647639	43.64463251

* not included since the sample didn't surpass the preconditioning cycle

#	Proben-ID	Determination of water content after submersion for 0 hours								
		Empty Eppendorf tube with drilled lid		Osmotic stress protocol (PEG immersion of specimens)		Eppendorf tube with frozen specimen (wet, -80°C)		Vacuum protocol, Eppendorf tube with freeze-dried specimen (dry, room temp.)		
		Date, Time	Weight (mg)	Start (date, time)	End (date, time)	Date, Time	Weight (mg)	Start (date, time)	End (date, time)	Weight (mg)
1	L69-vest	31.01.2024, 8:00	1010,11	13.02.2024, 13:00	13.02.2024, 13:00	13.02.2024, 13:00	1053,43	14.02.2024, 09:00	16.02.2024, 13:00	1018,21
2	L92-vest		1007,02				1023,28			1009,79
3	L65-vest		1003,65				1025,26			1011,62
4	M22-vest		1005,29				1031,30			1015,31
5	L40-vest		1006,42				1023,66			1015,04
6	M43-pal		1004,93				1030,29			1010,60
7	L85-pal		1007,96				1036,41			1013,45
8	M33-pal		1003,23				1028,65			1013,08
9	M22-pal		1006,69				1016,86			1010,31
10	L43-pal		1009,53				1045,28			1016,84
11	L82-pal		1005,48				1020,44			1009,02
12	L44-pal		1007,54				1030,90			1014,41
13										
14										
15										
Median			**1006,56**				**1029,47**			**1013,27**
Mean			**1006,49**				**1030,48**			**1013,14**
Standard dev.			**2,03**				**9,99**			**2,80**

#	Proben-ID	Determination of water content after submersion for 8 hours: 10% PEG								
		Empty Eppendorf tube with drilled lid		Osmotic stress protocol (PEG immersion of specimens)		Eppendorf tube with frozen specimen (wet, -80°C)		Vacuum protocol, Eppendorf tube with freeze-dried specimen (dry, room temp.)		
		Date, Time	Weight (mg)	Start (date, time)	End (date, time)	Date, Time	Weight (mg)	Start (date, time)	End (date, time)	Weight (mg)
1	L69-vest	13.03.2024, 16:00	1006,41	14.03.2024, 08:00	14.03.2024, 16:00	14.03.2024, 19:00	1049,72	15.03.2024, 14:00	18.03.2024, 15:00	1014,10
2	L92-vest		1004,40				1045,49			1017,76
3	L65-vest		1005,27				1054,30			1022,04
4	M22-vest		1007,39				1028,48			1013,71
5	L40-vest		1007,21				1029,82			1012,97
6	M43-pal		1006,81				1062,46			1025,15
7	L85-pal		1004,39				1036,45			1010,14
8	M33-pal		1003,73				1027,82			1010,47
9	M22-pal		1008,52				1034,91			1014,15
10	L43-pal		1009,21				1039,48			1016,08
11	L82-pal		1003,56				1042,81			1009,05
12	L44-pal		1007,34				1050,14			1029,96
13										
14										
15										
Median			**1006,61**				**1041,15**			**1014,13**
Mean			**1006,19**				**1041,82**			**1016,30**
Standard dev.			**1,80**				**10,52**			**6,14**

#	Proben-ID	Determination of water content after submersion for 12 hours: 10% PEG								
		Empty Eppendorf tube with drilled lid		Osmotic stress protocol (PEG immersion of specimens)		Eppendorf tube with frozen specimen (wet, -80°C)		Vacuum protocol, Eppendorf tube with freeze-dried specimen (dry, room temp.)		
		Date, Time	Weight (mg)	Start (date, time)	End (date, time)	Date, Time	Weight (mg)	Start (date, time)	End (date, time)	Weight (mg)
1	L69-vest	13.03.2024, 16:00	1008,90	14.03.2024, 08:00	14.03.2024, 20:00	14.03.2024, 21:00	1046,47	15.03.2024, 14:00	18.03.2024, 15:00	1016,24
2	L92-vest		1002,25				1039,21			1014,26
3	L65-vest		1006,03				1082,29			1031,97
4	M22-vest		1007,51				1063,32			1024,86
5	L40-vest		1007,34				1061,75			1017,37
6	M43-pal		1005,57				1046,93			1013,69
7	L85-pal		1008,19				1039,64			1014,56
8	M33-pal		1004,10				1026,50			1011,90
9	M22-pal		1008,29				1048,01			1016,67
10	L43-pal		1006,96				1037,31			1014,15
11	L82-pal		1010,24				1055,99			1021,66
12	L44-pal		1006,07				1047,91			1014,90
13										
14										
15										
Median			**1007,15**				**1047,42**			**1015,57**
Mean			**1006,79**				**1049,61**			**1017,69**
Standard dev.			**2,08**				**14,02**			**5,52**

#	Proben-ID	Determination of water content after submersion for 24 hours: 10% PEG								
		Empty Eppendorf tube with drilled lid		Osmotic stress protocol (PEG immersion of specimens)		Eppendorf tube with frozen specimen (wet, -80°C)		Vacuum protocol, Eppendorf tube with freeze-dried specimen (dry, room temp.)		
		Date, Time	Weight (mg)	Start (date, time)	End (date, time)	Date, Time	Weight (mg)	Start (date, time)	End (date, time)	Weight (mg)
1	L69-vest	13.03.2024, 16:00	1006,93	13.03.2024, 16:00	14.03.2024, 16:00	14.03.2024, 19:00	1028,35	15.03.2024, 14:00	18.03.2024, 15:00	1012,80
2	L92-vest		1005,71				1035,56			1012,45
3	L65-vest		1006,35				1038,54			1013,94
4	M22-vest		1007,01				1036,70			1016,22
5	L40-vest		1005,46				1030,88			1009,04
6	M43-pal		1003,77				1030,15			1009,57
7	L85-pal		1010,33				1039,85			1015,21
8	M33-pal		1007,08				1054,96			1024,66
9	M22-pal		1010,29				1038,37			1016,44
10	L43-pal		1008,51				1033,44			1015,49
11	L82-pal		1007,18				1037,73			1012,93
12	L44-pal		1006,13				1034,49			1013,04
13										
14										
15										
Median			**1006,97**				**1036,13**			**1013,49**
Mean			**1007,06**				**1036,59**			**1014,32**
Standard dev.			**1,82**				**6,54**			**3,84**

#	Proben-ID	Determination of water content after submersion for 8 hours 5% PEG								
		Empty Eppendorf tube with drilled lid		Osmotic stress protocol (PEG immersion of specimens)		Eppendorf tube with frozen specimen (wet, -80°C)		Vacuum protocol, Eppendorf tube with freeze-dried specimen (dry, room temp.)		
		Date, Time	Weight (mg)	Start (date, time)	End (date, time)	Date, Time	Weight (mg)	Start (date, time)	End (date, time)	Weight (mg)
1	L69-vest	31.01.2024, 8:00	1008,59	12.02.2024, 11:00	12.02.2024, 19:00	13.02.2024, 13:00	1090,63	14.02.2024, 09:00	16.02.2024, 13:00	1020,61
2	L92-vest		1009,84				1042,98			1015,67
3	L65-vest		1011,37				1034,42			1018,70
4	M22-vest		1007,22				1024,79			1014,30
5	L40-vest		1010,18				1021,13			1012,50
6	M43-pal		1008,92				1043,17			1015,33
7	L85-pal		1008,70				1020,41			1010,55
8	M33-pal		1005,34				1061,85			1026,82
9	M22-pal		1008,06				1028,74			1014,50
10	L43-pal		1009,32				1049,68			1016,60
11	L82-pal		1007,84				1025,14			1011,62
12	L44-pal		1005,95				1041,53			1012,66
13										
14										
15										
Median			**1008,65**				**1037,98**			**1014,92**
Mean			**1008,44**				**1040,37**			**1015,82**
Standard dev.			**1,64**				**19,37**			**4,32**

#	Proben-ID	Determination of water content after submersion for 12 hours 5% PEG								
		Empty Eppendorf tube with drilled lid		Osmotic stress protocol (PEG immersion of specimens)		Eppendorf tube with frozen specimen (wet, -80°C)		Vacuum protocol, Eppendorf tube with freeze-dried specimen (dry, room temp.)		
		Date, Time	Weight (mg)	Start (date, time)	End (date, time)	Date, Time	Weight (mg)	Start (date, time)	End (date, time)	Weight (mg)
1	L69-vest	31.01.2024, 8:00	1005,72	12.02.2024, 20:00	13.02.2024, 08:00	13.02.2024, 13:00	1051,37	14.02.2024, 09:00	16.02.2024, 13:00	1014,19
2	L92-vest		1002,62				1067,49			1012,50
3	L65-vest		1007,27				1045,34			1014,54
4	M22-vest		1005,67				1050,71			1020,91
5	L40-vest		1009,05				1049,97			1018,96
6	M43-pal		1007,12				1037,53			1011,72
7	L85-pal		1006,58				1063,88			1018,78
8	M33-pal		1006,77				1048,79			1014,97
9	M22-pal		1010,11				1044,56			1021,78
10	L43-pal		1002,42				1027,35			1006,69
11	L82-pal		1005,01				1033,07			1008,92
12	L44-pal		1005,78				1041,23			1013,81
13										
14										
15										
Median			**1006,18**				**1047,07**			**1014,37**
Mean			**1006,18**				**1046,77**			**1014,81**
Standard dev.			**2,14**				**11,03**			**4,43**

#	Proben-ID	Determination of water content after submersion for 24 hours 5% PEG								
		Empty Eppendorf tube with drilled lid		Osmotic stress protocol (PEG immersion of specimens)		Eppendorf tube with frozen specimen (wet, -80°C)		Vacuum protocol, Eppendorf tube with freeze-dried specimen (dry, room temp.)		
		Date, Time	Weight (mg)	Start (date, time)	End (date, time)	Date, Time	Weight (mg)	Start (date, time)	End (date, time)	Weight (mg)
1	L69-vest	31.01.2024, 8:00	1002,35	08.02.2024, 16:00	09.02.2024, 16:00	13.02.2024, 13:00	1050,52	14.02.2024, 09:00	16.02.2024, 13:00	1014,17
2	L92-vest		1008,19				1029,59			1012,42
3	L65-vest		1008,24				1021,66			1011,73
4	M22-vest		1008,60				1023,96			1016,54
5	L40-vest		1005,87				1036,49			1010,59
6	M43-pal		1004,97				1043,51			1029,39
7	L85-pal		1002,31				1018,74			1007,03
8	M33-pal		1003,83				1037,39			1011,44
9	M22-pal		1007,03				1033,05			1016,22
10	L43-pal		1005,65				1036,51			1012,17
11	L82-pal		1003,47				1021,81			1008,32
12	L44-pal		1009,14				1059,16			1028,47
13										
14										
15										
Median			**1005,76**				**1034,77**			**1012,30**
Mean			**1005,80**				**1034,37**			**1014,87**
Standard dev.			**2,35**				**11,81**			**6,82**

#	Proben-ID	Determination of water content after submersion for 8 hours 2.5% PEG								
		Empty Eppendorf tube with drilled lid		Osmotic stress protocol (PEG immersion of specimens)		Eppendorf tube with frozen specimen (wet, -80°C)		Vacuum protocol, Eppendorf tube with freeze-dried specimen (dry, room temp.)		
		Date, Time	Weight (mg)	Start (date, time)	End (date, time)	Date, Time	Weight (mg)	Start (date, time)	End (date, time)	Weight (mg)
1	L69-vest	26.03.2024, 16:00	1005,68	27.03.2024, 07:30	27.03.2024, 15:30	27.03.2024, 19:00	1030,67	02.04.2024, 15:00	05.04.2024, 09:00	1010,26
2	L92-vest		1006,08				1054,77			1019,15
3	L65-vest		1005,92				1041,95			1020,16
4	M22-vest		1002,87				1054,10			1018,56
5	L40-vest		1007,27				1039,00			1012,11
6	M43-pal		1009,93				1074,85			1021,95
7	L85-pal		1005,50				1050,59			1012,65
8	M33-pal		1005,62				1030,33			1008,72
9	M22-pal		1002,65				1044,07			1010,10
10	L43-pal		1010,62				1072,78			1017,02
11	L82-pal		1001,66				1028,16			1005,14
12	L44-pal		1008,97				1039,68			1014,44
13										
14										
15										
Median			**1005,80**				**1043,01**			**1013,55**
Mean			**1006,06**				**1046,75**			**1014,19**
Standard dev.			**2,70**				**14,76**			**4,99**

#	Proben-ID	Determination of water content after submersion for 12 hours 2.5% PEG								
		Empty Eppendorf tube with drilled lid		Osmotic stress protocol (PEG immersion of specimens)		Eppendorf tube with frozen specimen (wet, -80°C)		Vacuum protocol, Eppendorf tube with freeze-dried specimen (dry, room temp.)		
		Date, Time	Weight (mg)	Start (date, time)	End (date, time)	Date, Time	Weight (mg)	Start (date, time)	End (date, time)	Weight (mg)
1	L69-vest	26.03.2024, 16:00	1007,73	27.03.2024, 07:30	27.03.2024, 19:30	02.04.2024, 14:00	1018,40	02.04.2024, 15:00	05.04.2024, 09:00	1008,23
2	L92-vest		1006,02				1028,89			1011,16
3	L65-vest		1006,01				1016,15			1007,59
4	M22-vest		1007,76				1047,35			1018,33
5	L40-vest		1009,04				1021,85			1010,38
6	M43-pal		1003,66				1026,70			1007,81
7	L85-pal		1010,75				1030,16			1014,73
8	M33-pal		1005,39				1021,63			1008,92
9	M22-pal		1003,01				1019,47			1006,81
10	L43-pal		1003,73				1031,39			1009,76
11	L82-pal		1006,91				1020,18			1008,64
12	L44-pal		1008,21				1024,78			1013,46
13										
14										
15										
Median			**1006,47**				**1023,32**			**1009,34**
Mean			**1006,52**				**1025,58**			**1010,49**
Standard dev.			**2,24**				**8,05**			**3,28**

#	Proben-ID	Determination of water content after submersion for 24 hours 2.5% PEG								
		Empty Eppendorf tube with drilled lid		Osmotic stress protocol (PEG immersion of specimens)		Eppendorf tube with frozen specimen (wet, -80°C)		Vacuum protocol, Eppendorf tube with freeze-dried specimen (dry, room temp.)		
		Date, Time	Weight (mg)	Start (date, time)	End (date, time)	Date, Time	Weight (mg)	Start (date, time)	End (date, time)	Weight (mg)
1	L69-vest	26.03.2024, 16:00	1006,08	26.03.2024, 17:00	27.03.2024, 17:00	27.03.2024, 19:00	1028,20	02.04.2024, 15:00	05.04.2024, 09:00	1009,88
2	L92-vest		1008,72				1048,12			1016,59
3	L65-vest		1004,57				1037,09			1022,52
4	M22-vest		1006,78				1035,40			1014,20
5	L40-vest		1007,65				1056,78			1014,77
6	M43-pal		1005,75				1062,15			1019,40
7	L85-pal		1005,83				1043,09			1013,41
8	M33-pal		1008,69				1029,82			1012,93
9	M22-pal		1009,79				1044,08			1019,41
10	L43-pal		1009,54				1034,43			1013,71
11	L82-pal		1010,15				1034,66			1016,28
12	L44-pal		1001,75				1071,41			1022,90
13										
14										
15										
Median			**1007,22**				**1040,09**			**1015,53**
Mean			**1007,11**				**1043,77**			**1016,33**
Standard dev.			**2,37**				**12,95**			**3,83**